

Special Issue: Ribosomes & Translation

Feature Review

Structural Insights into the Mechanism of Scanning and Start Codon Recognition in Eukaryotic Translation Initiation

Alan G. Hinnebusch^{1,*}

Initiation of translation on eukaryotic mRNAs generally follows the scanning mechanism, wherein a preinitiation complex (PIC) assembled on the small (40S) ribosomal subunit and containing initiator methionyl tRNA_i (Met-tRNA_i) scans the mRNA leader for an AUG codon. In a current model, the scanning PIC adopts an open conformation and rearranges to a closed state, with fully accommodated Met-tRNA_i, upon AUG recognition. Evidence from recent high-resolution structures of PICs assembled with different ligands supports this model and illuminates the molecular functions of eukaryotic initiation factors eIF1, eIF1A, and eIF2 in restricting to AUG codons the transition to the closed conformation. They also reveal that the eIF3 complex interacts with multiple functional sites in the PIC, rationalizing its participation in numerous steps of initiation.

Translation Initiation by the Scanning Mechanism

Translation initiation is the process of decoding the AUG start codon in mRNA by methionyl initiator tRNA (Met-tRNA_i). Most eukaryotic mRNAs are translated by a scanning mechanism, where the small (40S) ribosomal subunit is first loaded with Met-tRNA_i in a ternary complex (TC) with GTP-bound eukaryotic initiation factor 2 (eIF2) in a reaction promoted by eIF1, eIF1A, eIF5, and the multisubunit eIF3. This 43S preinitiation complex (PIC) then attaches to the 5' end of mRNA – preactivated by association with eIF4F (consisting of m⁷G cap-binding protein eIF4E, scaffold subunit eIF4G, and DEAD-box helicase eIF4A) at the cap and poly(A)-binding protein bound to the poly(A) tail – to form the 48S PIC (Figure 1) [1]. The 5' untranslated region (5' UTR) is then scanned base-by-base for complementarity to the anticodon of Met-tRNA_i as successive triplets enter the peptidyl (P) decoding site of the 40S subunit. The first AUG encountered is favored as the start codon, but can be skipped if its surrounding sequence context does not conform to the 'Kozak' consensus, featuring a purine at position –3 and guanine at +4 relative to the AUG (at +1). AUG recognition triggers hydrolysis of GTP in the TC and release of eIF2–GDP from Met-tRNA_i, which is followed by joining of the large (60S) subunit, stimulated by eIF5B, to form an 80S initiation complex (Figure 1). The elongation phase of protein synthesis commences with decoding of the next triplet positioned in the ribosomal A-site (reviewed in [2–4]). The eIF4A in conjunction with other RNA helicases, including Ddx3 and Dhx29, uses the energy of ATP hydrolysis to unwind secondary structures that impede PIC attachment or threading of mRNA in single-stranded

Trends

Recent high-resolution structures of PICs reveal distinct conformations of the 40S subunit, (initiator) tRNA_i, and initiation factors indicative of different stages of the scanning mechanism for selecting AUG start codons.

An open PIC conformation features less tightly anchored mRNA and tRNA_i, and unobstructed binding of the gatekeeper molecule eIF1 – all features compatible with scanning.

In the closed PIC conformation, both mRNA and tRNA_i are locked into the decoding center, distorting eIF1 as a prelude to its release; and eIF1A stabilizes tRNA_i binding – all compatible with AUG selection.

eIF2 subunits encase tRNA_i within the TC; eIF2 β helps to retain eIF1 in the open complex, and eIF2 α interacts directly with 'context' mRNA nucleotides surrounding the AUG.

eIF3 effectively encircles the PIC and contacts various 40S functional sites, illuminating its multiple roles in stimulating PIC assembly, scanning, and AUG selection.

¹Laboratory of Gene Regulation and Development, Eunice Kennedy Shriver National Institute of Child Health and Human Development, National Institutes of Health, Bethesda, MD 20892, USA

*Correspondence: ahinnebusch@nih.gov
(A.G. Hinnebusch).

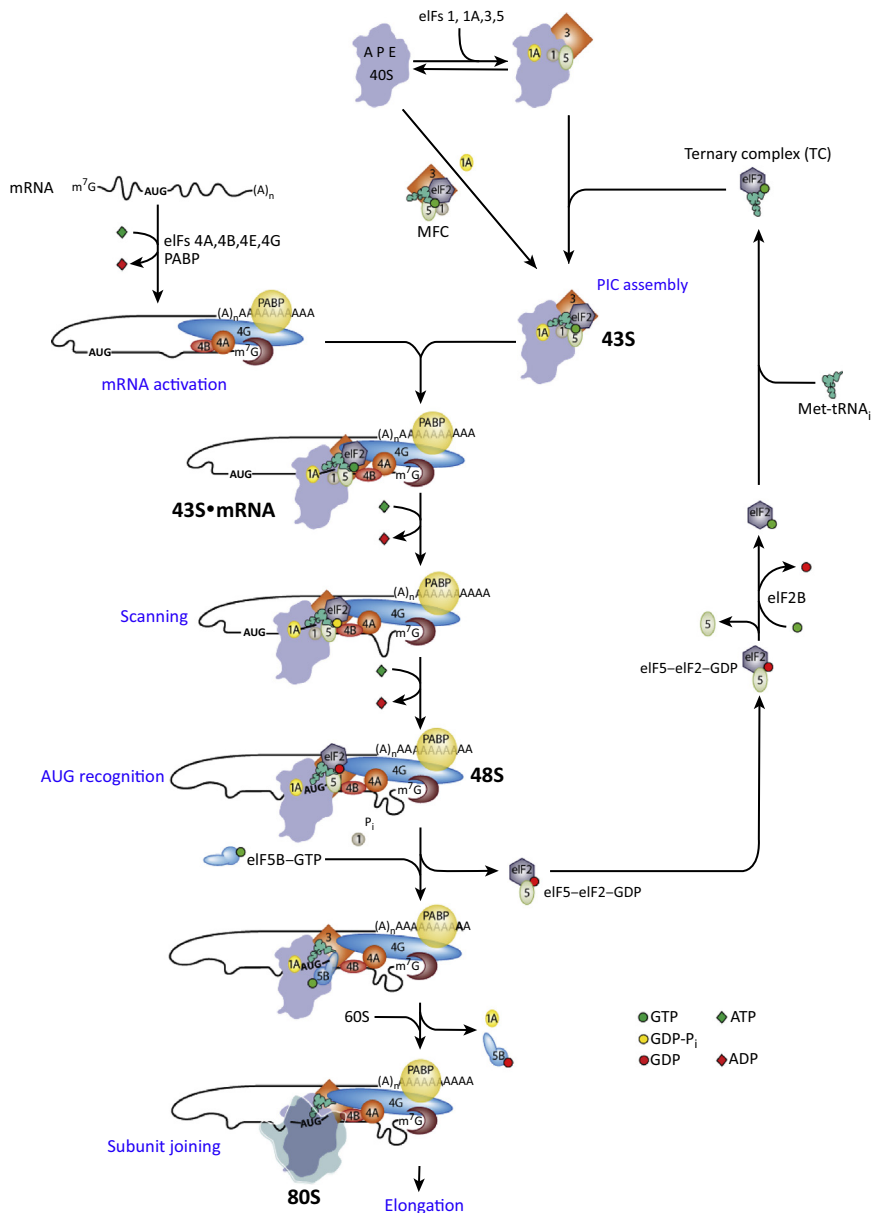


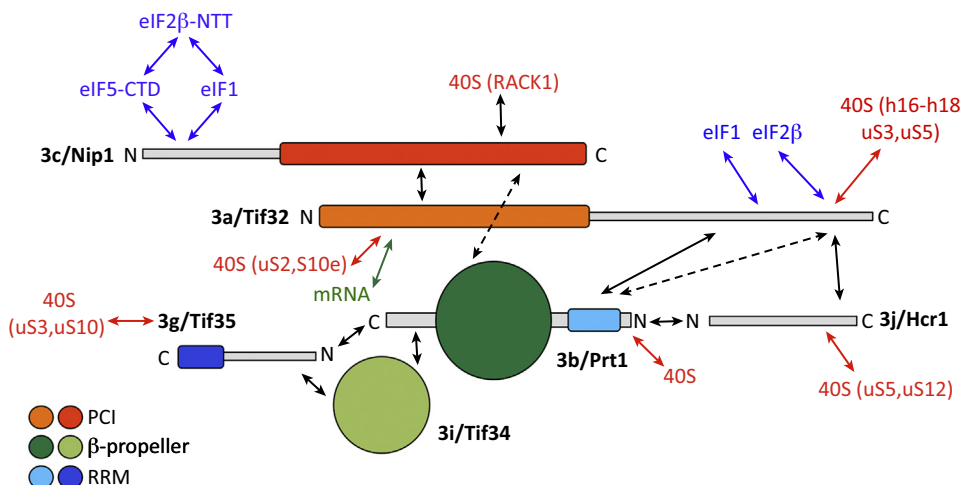
Figure 1. Model of the Scanning Mechanism of Eukaryotic Translation Initiation. The pathway is shown as a series of discrete steps starting with assembly of the 43S PIC, depicted as a single step via the MFC or as two separate steps, with eIFs 1, 1A, and 3 binding first and stimulating recruitment of TC and eIF5. The 43S PIC attaches near the 5'-cap of activated mRNA. Subsequent scanning of the mRNA is accompanied by GTP hydrolysis by the TC without release of P_i , which is triggered by recognition of the start codon and gated by eIF1 dissociation. GTP-bound eIF5B promotes joining of the 60S subunit to the PIC, with release of eIF5B-GDP and eIF1A to form the 80S IC, ready for the elongation phase of protein synthesis. eIF2-GDP released after subunit joining (in a complex with eIF5) is recycled back to eIF2-GTP by the exchange factor eIF2B (modified from [4]). Abbreviations: eIF, eukaryotic initiation factor; IC, initiation complex; MFC, multi-initiation factor complex; PIC, preinitiation complex; TC, eIF2-GTP-Met-tRNA_i ternary complex.

form through the 40S subunit, and to provide 5' to 3' directionality to the process. Factors eIF1, eIF1A, eIF2, eIF3, and eIF5 regulate scanning and AUG recognition by interacting directly with the 40S subunit or Met-tRNA_i [3], and their functions are the focus of this review.

elf3 is a multisubunit complex that participates throughout the initiation pathway, promoting 43S PIC assembly, 43S attachment to mRNA, scanning, and accurate start codon selection (for review, see [3,5]). It is the only factor that differs dramatically in structure between yeast and mammals: whereas mammalian elf3 (melf3) contains 13 subunits (a through m), yeast elf3 (yelf3) contains only five essential subunits, a/Tif32, b/Prt1, c/Nip1, g/Tif35, and i/Tif34, and one nonessential, substoichiometric subunit j/Hcr1. The subunit interactions deduced for yelf3 (Figure 2) are thought to exist in the more complicated melf3 complex. yelf3 also forms a larger, multi-initiation factor complex (MFC) by interacting directly with both elf1 and the elf5-C-terminal domain (CTD) via the 3c-N-terminal domain (NTD), and also with elf1 and the unstructured elf2 β -N-terminal tail (NTT) via the 3a-CTD [6–9] (Figure 2). The elf2 β -NTT, elf1, and elf5-CTD additionally interact with one another [9]. The MFC likely participates in recruitment of TC to 40S subunits (Figure 1) in yeast [7,8] and also in mammals [10]. Moreover, interaction of elf1 with the 3c-NTD [11,12] and the exchange of elf2 β -NTT/elf1 for elf2 β -NTT/elf5-CTD interactions [13] promotes accurate selection of AUG start codons *in vivo*. Thus, MFC formation both enhances PIC assembly and coordinates interactions among initiation factors in the transition between scanning and start codon recognition.

A Model for the Scanning Mechanism

Biochemical, genetic, and structural analyses have led to the following model for the mechanism of scanning (Figure 3; for reviews, see [3,4]). Factors elf1 and elf1A bind the 40S subunit near the P and A sites, respectively, and promote an open 40S conformation conducive to rapid loading of TC and mRNA scanning. TC is bound in a 'P_{OUT}' conformation, not fully engaged with the PIC, suitable for scanning successive triplets entering the P site. GTP hydrolysis by TC is stimulated by the GTPase activating protein (GAP) elf5 and the 40S subunit itself, but release of inorganic phosphate (P_i) from elf2-GDP-P_i is blocked at non-AUG codons by elf1. The open/P_{OUT} conformation is also promoted by the 'scanning enhancer' (SE) elements of the unstructured C-terminal tail (CTT) of elf1A, which occupies a portion of the P site, and by interaction of scanning inhibitor (SI) elements in the elf1A NTT with the CTD of elf5 and elf1



Trends in Biochemical Sciences

Figure 2. Interactions of Yeast elf3 Subunits. Linear depictions of yeast elf3 subunits with arrows showing established interactions with one another (black), other initiation factors in the MFC (blue), the 40S subunit (and specific 40S constituents in parenthesis) (red), and mRNA at the exit channel (green). The proteasome-COP9-initiation factor (PCI), β-propeller, and RRM domains, of known structure, within elf3 subunits are indicated by filled colored rectangles or circles (figure adapted from [64]; see [5] for review of interactions). Abbreviations: elf, eukaryotic initiation factor; MFC, multi-initiation factor complex; NTT, N-terminal tail; RRM, RNA recognition motif.

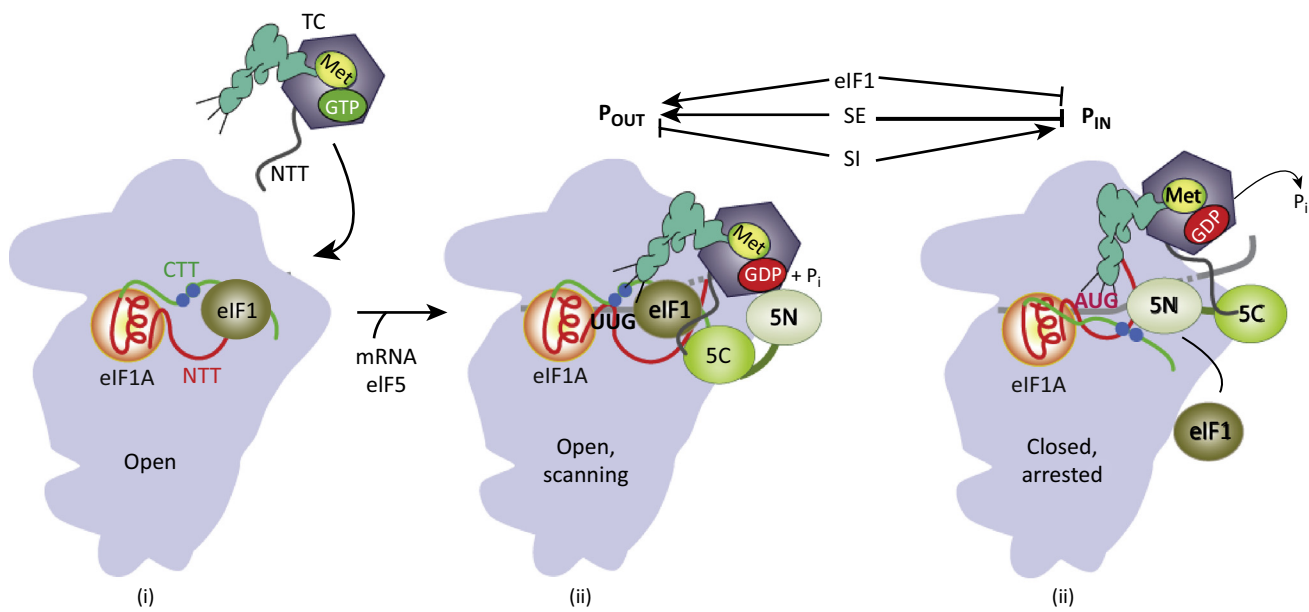


Figure 3. Model of Structural Rearrangements in the PIC Accompanying Start Codon Recognition. (i) Binding of eIF1 and eIF1A to the 40S subunit evokes an open conformation conducive to rapid TC binding, forming the 43S PIC. (ii) Following attachment to the mRNA, the 43S PIC scans the 5' UTR with the ASL of Met-tRNA_i not fully accommodated in the P site (P_{OUT}), owing to clashes with eIF1 and the unstructured CTT of eIF1A, but capable of sampling triplets for complementarity to the anticodon. The GAP domain in the eIF5-NTD (5N) stimulates GTP hydrolysis to produce GDP- P_i , but release of P_i is blocked. The unstructured NTT of eIF2 β interacts with eIF1, and the NTT of eIF1A interacts with the eIF5-CTD and eIF1 to stabilize this open conformation of the PIC. (iii) Base pairing between the anticodon and AUG codon promotes movement of the tRNA from the P_{OUT} to P_{IN} state, displacing eIF1 and the eIF1A-CTT from the P site. eIF1 dissociates from the 40S and the eIF1A-CTT moves into proximity with the eIF5-NTD, gating P_i release. The eIF2 β -NTT interacts with the eIF5-CTD, and the eIF1A-NTT interacts with the codon-anticodon helix, to stabilize the closed, scanning-incompatible conformation of the 40S subunit and P_{IN} state. As shown in the upper diagram, eIF1 and the scanning enhancer (SE) elements in the eIF1A-CTT (filled blue circles) promote P_{OUT} and the open PIC conformation (ii) while impeding the closed, P_{IN} conformation (iii). Scanning inhibitor (SI) elements in the eIF1A-NTT function oppositely. Abbreviations: 5' UTR, 5' untranslated region of mRNA; ASL, anticodon stem-loop of tRNA_i; CTD, C-terminal domain; CTT, C-terminal tail; eIF, eukaryotic initiation factor; GAP, GTPase activating protein; NTD, N-terminal domain; NTT, N-terminal tail; P, peptidyl decoding site of the 40S subunit; PIC, preinitiation complex; TC, eIF2-GTP-Met-tRNA_i ternary complex (modified from [4]).

[14]. Base pairing of Met-tRNA_i with an AUG triplet evokes dissociation of eIF1 from the 40S subunit, enabling more stable binding of Met-tRNA_i in a ' P_{IN} ' conformation and rearrangement to a closed conformation of the 40S restrictive for scanning. The eIF5-CTD interacts with the unstructured NTT of eIF2 β , which should disfavor partially overlapping eIF5-CTD interactions with eIF1, and the eIF1A CTT is ejected from the P site to allow functional interaction of its SE elements with eIF5-NTD. Dissociation of eIF1, followed by the eIF1A-CTT/eIF5-NTD interaction, gates P_i release, and eIF2-GDP dissociates from the PIC in a complex with eIF5 to leave Met-tRNA_i base paired with the AUG codon [3,4].

The multiple interactions of eIF3 with eIF1, eIF5-CTD, eIF2 β -NTT, and 40S constituents (Figure 2) provide the potential for eIF3 to influence the transition between the open/ P_{OUT} and closed/ P_{IN} conformations of the PIC; and, indeed, eIF3 mutations are known to alter the efficiency or fidelity of AUG recognition [5]. However, determining eIF3's precise roles in the scanning mechanism has been hampered by the lack of structural information about its location and interactions within the PIC. Progress in deciphering the molecular functions of eIF1, eIF1A, and the subunits of eIF2 has also been hindered by the absence of high-resolution structures of PICs containing all of these factors. As described in the following sections, recent structural characterization of reconstituted PICs captured in different stages of initiation has provided strong support for key tenets of the scanning model (Figure 3), and revealed how eIFs interact with one another, tRNA_i, mRNA, and the 40S subunit to control conformational changes in the

PIC that accompany the transition from scanning to initiation, and to limit this transition to AUG triplets. They also have revealed how eIF3 is anchored to the PIC in a way that enables its direct communication with the mRNA entry and exit sites of the 40S subunit and with various eIFs bound in the decoding center, illuminating eIF3's ability to modulate multiple steps of the initiation pathway.

Structure of TC

Met-tRNA_i is anchored to the scanning PIC in the TC with GTP-bound eIF2, an $\alpha/\beta/\gamma$ heterotrimer. The γ -subunit is related to the three-domain factor EF1A, which transfers charged tRNAs to the A site during translation elongation, featuring a GTP-binding pocket in the G domain. Though absent in eubacteria, archaea contain a similar factor, alF2, and crystal structures of alF2 subcomplexes [15–18] and archaeal TC (aTC) [19] provided detailed glimpses into how eukaryotic TC might be organized. More recently, eukaryotic TC was visualized in electron cryomicroscopy (cryo-EM) reconstructions of two partial yeast 48S PICs (py48S PIC and py48S-closed) [20,21] (Figure 4A). These PICs were assembled with eIF1, eIF1A, and uncapped, unstructured model mRNA, in addition to TC, using the yeast reconstituted system [22]. Watson–Crick (W–C) base pairing of the Met-tRNA_i anticodon with the AUG codon indicated P_{IN} conformations in both structures.

Comparing free aTC with 48S-bound yeast TC reveals important structural differences involving the α -subunit (Figure 4B). Whereas (archaeal) alF2 α domains 1 and 2 (D1–2) interact with the tRNA elbow, they are dramatically rearranged in the yeast py48S complexes with D1 contacting the anticodon stem loop (ASL) and D2 interacting with the D-/T-loops of tRNA_i, slightly distorting the T-loop [20]. This distortion might account for the increased initiation at near-cognate UUG codons in yeast (Sui⁺ phenotype) conferred by a T-loop mutation [23] if the substitution reduces the energetic cost of the distortion. eIF2 α -D3 interacts with the tRNA_i acceptor arm much as in the aTC (Figure 4B). The reorientation of eIF2 α D1–2 was also observed in a cryo-EM structure of a partial mammalian 43S PIC lacking mRNA but containing RNA helicase Dhx29 [24], and is consistent with alF2 crystal structures showing that alF2 α domains D1–2 are mobile elements attached to a rigid core composed of alF2 α -D3, alF2 γ , and helix 1 of alF2 β [15–18].

In the py48S PIC, eIF2 α -D1 is found in essentially the same E-site location that would be occupied by the ASL of an elongator tRNA when Met-tRNA_i occupies the P site. eIF2 α -D1 contacts 40S protein uS7 (Rps5 in yeast; Figure 4C) [20], consistent with both crosslinking data from a mammalian PIC [25] and results implicating the yeast uS7 β -hairpin, near the eIF2 α -D1/uS7 interface, in stabilizing the P_{IN} mode of TC binding [26]. Arg residues in an unstructured loop of eIF2 α -D1 interact with mRNA nucleotides upstream of the AUG, including the key –3 position of the Kozak consensus [20]. This interaction agrees with crosslinking of eIF2 α to the –3 nucleotide in reconstituted mammalian PICs and biochemical data indicating that meIF2 α stabilizes 48S PICs and mediates the stimulatory effect of a –3 purine on 48S assembly [27]. It is unknown, however, whether the eIF2 α Arg residues actually 'sense' favorable Kozak context, for example, by distinguishing purine from pyrimidine bases at the –3 nucleotide.

Thus, these structural data revealed how eIF2 γ and the three domains of eIF2 α form an extensive interface with Met-tRNA_i in the TC, which appears to be dynamic and capable of distorting tRNA_i conformation within the PIC; and they also unveiled direct contacts of eIF2 α -D1 with the key –3 nucleotide in mRNA.

Interactions of tRNA_i with P Site Residues Stabilize the P_{IN} Conformation

Comparing the pm43S PIC (lacking mRNA) [24] with the py48S PIC [20] suggested that the tRNA_i is inserted \sim 7 Å less deeply in the P site of pm43S PIC, consistent with a P_{OUT} state [20]. However, examining the pm43S complex at higher resolution [28] indicates that tRNA_i is not

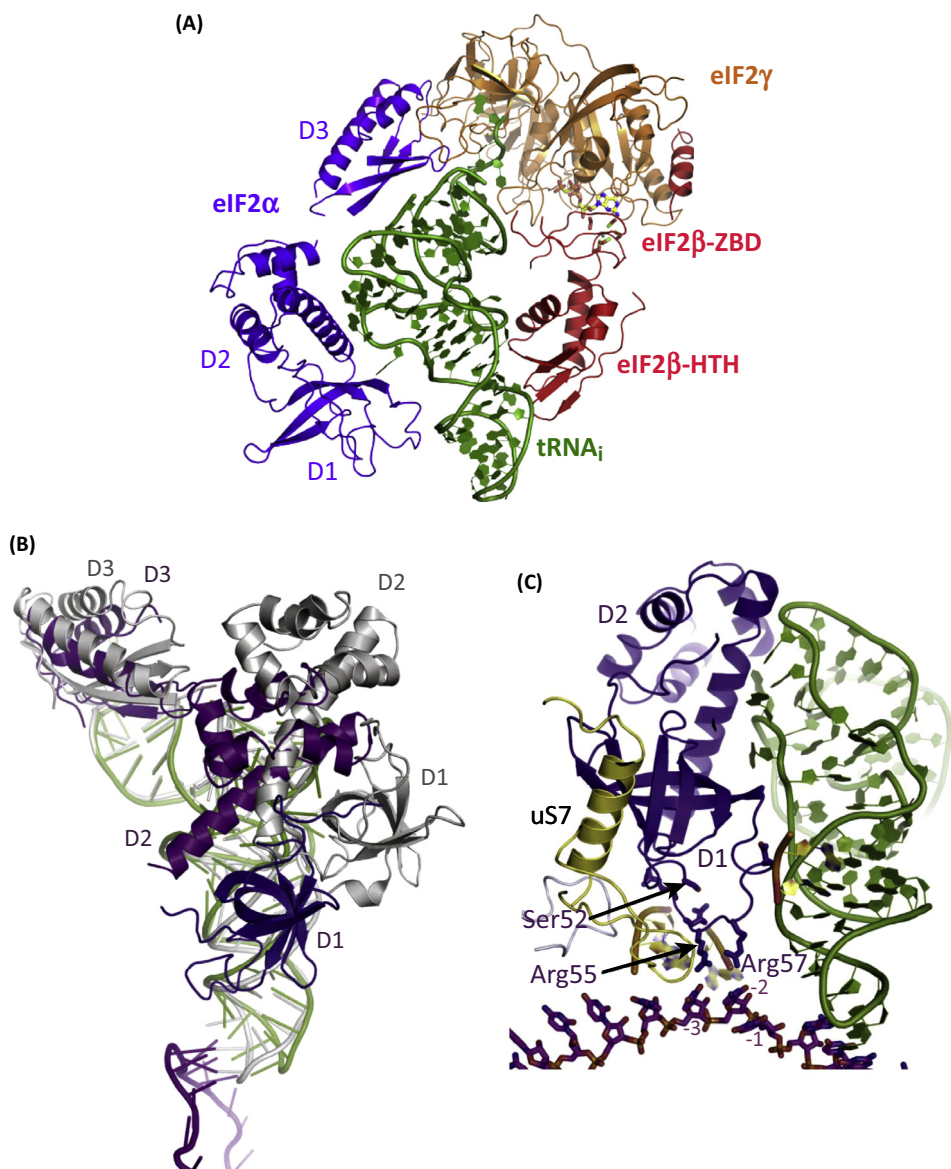
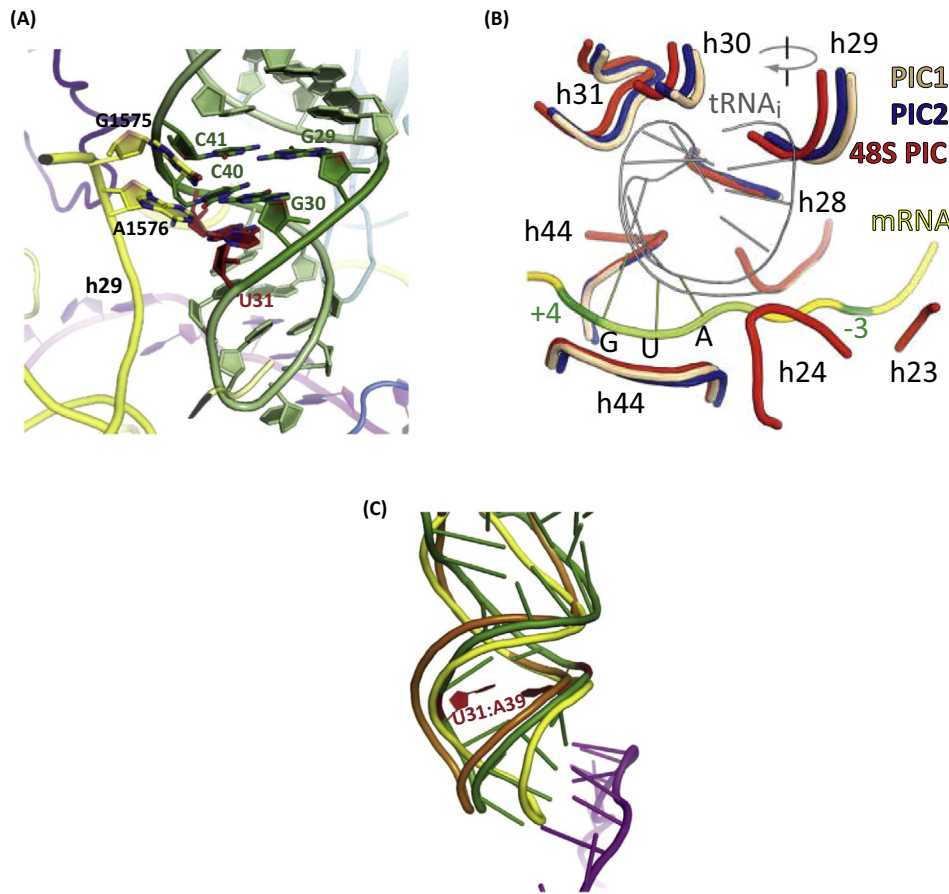


Figure 4. Structure of the TC in Partial Yeast 48S PICs and Comparison with Free Archaeal TC. (A) Ribbons depictions of the yeast TC in py48S-closed (PDB 3JAP; provided by Jose L. Llacer). Abbreviations: ZBD, zinc-binding domain; HTH, helix-turn-helix. (B) Overlay of TC in py48S (PDB 3J81) and free aTC (PDB 3V11) illustrating rearrangement of domains D1 and D2 in TC (shades of purple) versus aTC (shades of gray). (C) eIF2 α -D1 occupies the position of an E-site tRNA in py48S (PDB 3J81), interacting with mRNA immediately 5' of the AUG and uS7 (Panels B and C reproduced from [20]). Abbreviations: eIF, eukaryotic initiation factor; PIC, preinitiation complex; TC, eIF2-GTP-Met-tRNA_i ternary complex.

inserted less deeply, but rather occupies the P site differently in the two complexes, owing to angular rotation of the entire TC relative to the head and body of the 40S subunit (Yaser Hashem, personnel communication). The P_{IN} location of tRNA_i in the py48S structure enables interactions of the ASL with rRNA residues in the P site, helping to account for the enhanced stability of the P_{IN} state demonstrated biochemically [29,30]. These P-site residues include G1575/A1576 of helix 29 (h29) that make minor groove interactions with the first two of three highly conserved G-C base pairs in the tRNA_i ASL (Figure 5A) [20], an interaction supported by



Trends in Biochemical Sciences

Figure 5. Met-tRNAi^{Met} Binding in the P_{in} Conformation. (A) Contacts between h29 residues G1575/A1576 with the ASL of Met-tRNAi^{Met} in py48S (PDB 3J81). (B) Superposition of 18S rRNA helices in the P site in the crystal structures of mammalian 40S-eIF1 (PIC1, pink), 40S-eIF1-eIF1A (PIC2, blue), and 40S-mRNA-tRNA_i-eIF1A (48S PIC, red) complexes (Reproduced from [35]). (C) Distortion of the ASL on codon-anticodon base pairing evident in py48S (green; PDB 3J81) and pm48S (orange) [35] compared with pm43S (yellow) [24]. The Sui⁻ ASL substitution U31:A39 present in py48S, which elevates UUG initiation *in vivo*, is highlighted in red (Panels A & C reproduced from [20]). Abbreviations: ASL, anticodon stem loop; eIF, eukaryotic initiation factor; PIC, preinitiation complex.

increased sensitivity of G1575/A1576 to hydroxyl radical cleavage in py48S complexes containing a near-cognate AUC versus AUG triplet [31]. Comparing the crystal structures of a partial mammalian 48S PIC (pm48S PIC), which contains eIF1A and tRNA_i base paired to AUG in mRNA, to a mammalian 40S-eIF1-eIF1A complex (lacking mRNA and tRNA_i) also revealed rearrangements of h29 and h24 that should lock tRNA_i into the P site, whereas a predicted clash between the ASL and h31 is avoided (Figure 5B).

In accordance with these structural findings, substituting the first and third ASL G-C base pairs with other W-C base pairs eliminates the stabilizing effect of AUG on TC binding to reconstituted yeast PICs [32], impairs translation in mammalian extracts [33], and destabilizes reconstituted mammalian PICs following GTP hydrolysis in the TC [34]. Furthermore, most purine-purine and pyrimidine-pyrimidine mismatches at the first two ASL base pairs are lethal in yeast, as are most substitutions of h29 residues G1575/A1576, which impair AUG recognition in viable cells coexpressing wild-type (WT) rRNA [23]. Interestingly, while not lethal, pyrimidine-pyrimidine mismatches at the third ASL G-C base pair increase initiation accuracy

by discriminating against near-cognate UUG codons, and destabilize TC binding to reconstituted yeast 48S PICs even with an AUG start codon, whereas W–C replacements of this base pair elevate UUG initiation and confer hyperstable TC binding to the PIC *in vitro* [23]. One such Sui[−] tRNA_i variant (U31:A39), along with a Sui[−] variant of eIF2, was employed in assembling the py48S PIC for structural analysis to help stabilize the P_{IN} state [20]. The ASL conformation in py48S [20] and pm48S [35] is altered from that in pm43S [24], which allows W–C pairing with the start codon while avoiding a clash with the mRNA (Figure 5C), and the U31:A39 substitution might facilitate this conformational change to allow increased initiation at near-cognate codons.

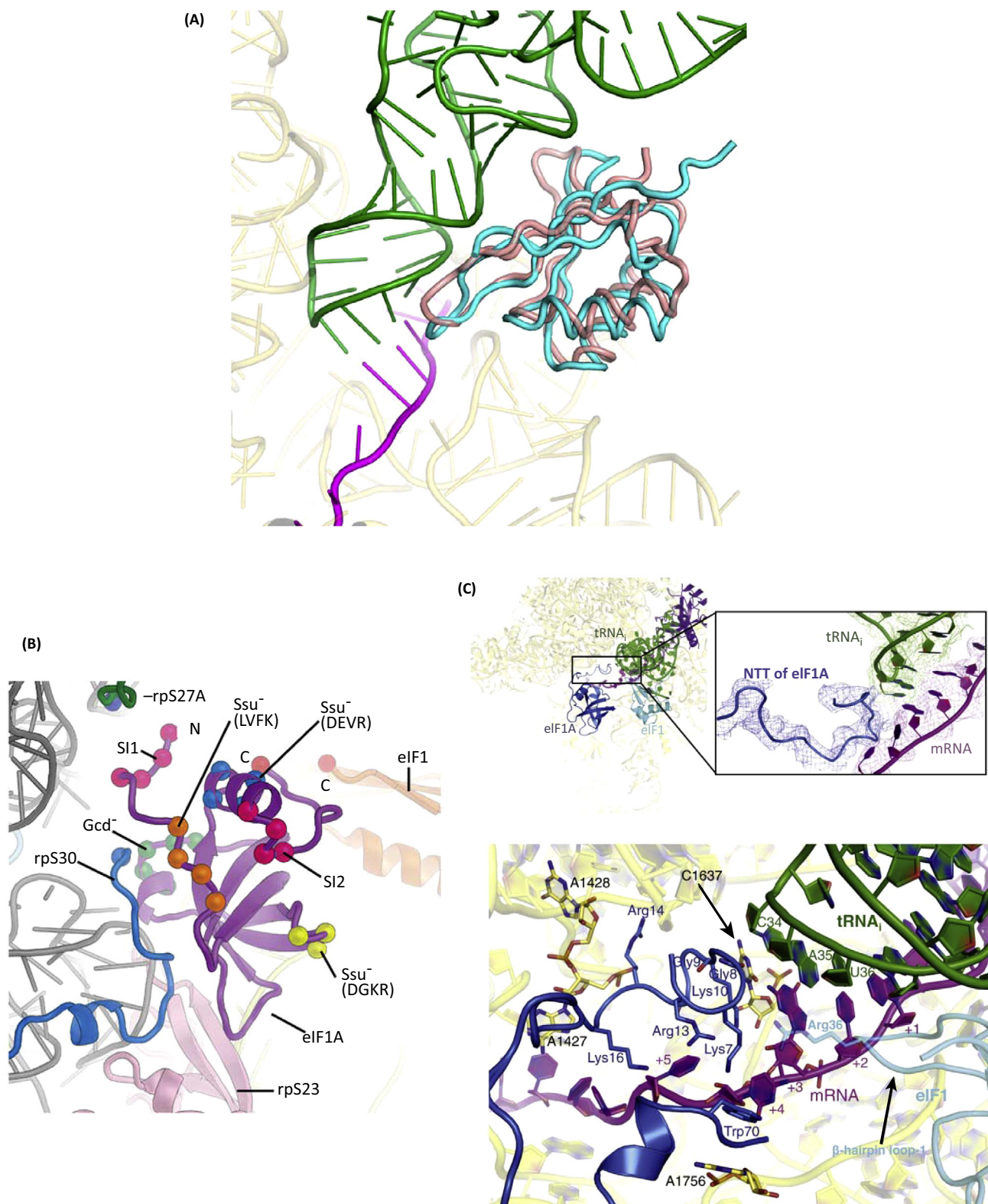
Comparing the mammalian pm48S and 40S–eIF1–eIF1A complexes revealed a ~3° rotation of the 40S head relative to the body [35]; and similar findings were made comparing the yeast py48S and 40S–eIF1–eIF1A PICs [20]. Helix 28 is the pivot point for head rotation, which might explain why h28 substitutions in yeast appear to destabilize the P_{IN} state and allow bypass of AUG codons during scanning (leaky scanning) [36]. Comparing the mammalian 40S–eIF1–eIF1A and 40S–eIF1 complexes [35], and the yeast 40S–eIF1–eIF1A with free 40S [20], indicates that simultaneous binding of eIF1 and eIF1A also promotes head rotation relative to 40S–eIF1 or empty 40S. This change in 40S structure could be instrumental in eIF1/eIF1A enhancement of TC binding during 43S assembly, through changes in the position of P-site helices (Figure 5B). However, a more recent structure discussed below, py48S-open, reveals direct interactions of eIF2 β with both eIF1 and eIF1A that could also promote TC binding in the open conformation [21].

These structural data showed that progressive rotation of the 40S head relative to the body is triggered by initiation factors and brings 18S rRNA residues in the P site into direct contact with the ASL of tRNA_i, to establish a stable P_{IN} state.

tRNA_i Clashes with eIF1 in the P_{IN} State

The crystal structure of a *Tetrahymena* 40S–eIF1 complex [37] revealed eIF1 bound to the 40S platform near the P site, consistent with directed hydroxyl radical cleavage (DHRC) mapping of eIF1 in reconstituted mammalian PICs [38]. It was predicted that eIF1 would clash with tRNA_i bound in the canonical P/P state [37]. This expectation was extended by overlaying the crystal structures of the mammalian 40S–eIF1–eIF1A and m48S PIC, which predicted clashes of the ASL with loop-1, and the tRNA_i D-stem with loop-2 of eIF1. These predictions were supported by comparing the py48S, containing both TC and eIF1, with a 40S–eIF1–eIF1A complex lacking TC, revealing a slight displacement of eIF1 on the 40S and altered conformations of loops 1 and 2 in py48S that avoids the predicted clashes with tRNA_i [20] (Figure 6A). It was suggested that the high concentration of eIF1 used to assemble py48S maintained the factor on the 40S subunit despite the P_{IN} conformation of tRNA_i expected to dislodge eIF1.

Basic residues in eIF1 loop-1 are near the rRNA backbone in h44 and mediate stable eIF1 binding, as Ala substitutions of these residues weaken 40S binding by eIF1 *in vitro* and confer the hypoaccuracy Sui[−] phenotype, indicating improper eIF1 dissociation from the PIC at UUG codons [39]. The remodeling of (WT) loop-1 in the py48S PIC should disrupt certain interactions anchoring eIF1 to the 40S, leaving only contact between (yeast eIF1) Arg-36 and the codon–anticodon duplex [20]. Conformational changes in h44 near the eIF1 binding site, detected when comparing pm48S and mammalian 40S–eIF1–eIF1A complexes, might also weaken eIF1 binding and help provoke its dissociation from the PIC on AUG recognition [35]. Together, these findings plausibly explain how eIF1 can both promote recruitment of TC and coexist with tRNA_i in the P_{OUT} conformation of the 43S PIC, while impeding accommodation of tRNA_i in the P_{IN} state via steric clashes and thereby oppose transition to P_{IN} at non-AUG codons. They also suggest how a perfect codon–anticodon duplex formed at AUG could provide the energy required to overcome the clash with eIF1 and evoke the distortion and displacement of eIF1 that



weakens its contacts/affinity for the 40S. This model also fits with the previous suggestion that eIF1 moves to a new location in the PIC on AUG recognition prior to its dissociation [40].

The eIF1A NTT Stabilizes the Codon–Anticodon Helix

The globular domain of eIF1A binds to the 40S A site, as demonstrated by DHRC mapping in mammalian PICs [41] and crystal structures of 40S–eIF1–eIF1A complexes from *Tetrahymena* [42] and mammals [35]. The helical domain and associated NTT and CTT of eIF1A project from the globular domain bound to the 40S body, and the NTT interacts with Rps27A (Rps31 in yeast) in the 40S head [35, 42] (Figure 6B). The ability of eIF1A to bridge the 40S head and body could influence the mRNA binding cleft formed at the head–body interface 3' of the AUG in the mRNA entry channel. Much of the NTT and most of the CTT were not resolved in crystal structures, but their trajectories were consistent with predictions from DHRC mapping of projections into the P site at locations compatible (NTT) or clashing (CTT) with tRNA_i in a P/P orientation [41]. However, all but four NTT residues were resolved in the py48S PIC, revealing interactions of basic residues with rRNA in the 40S head and mRNA in the entry channel and also direct interactions with the codon–anticodon helix (Figure 6C). Thus, the NTT should stabilize 40S head–body connections that constrict the mRNA binding cleft, and the P_{IN} conformation of tRNA_i binding. These results help to account for findings that substitutions of yeast eIF1A residues in the SI elements of the eIF1A NTT, or helix α 2 that helps to anchor the NTT, destabilize the closed conformation and shift the system toward the open, scanning state, as indicated by reduced affinity of eIF1A for the PIC, increased rate of TC loading, and decreased rate of 60S subunit joining *in vitro* – all hallmarks of the open complex. Consistently, these SI mutations also suppress initiation at near-cognate UUG codons in Ssu[−] mutants (the Ssu[−] hyperaccuracy phenotype, Figure 6B) and increase bypass of the poor-context AUG of eIF1 mRNA and the AUG codon of an upstream open-reading frame (uORF) by the scanning PIC [43–45].

Mutations in the SE elements of the eIF1A CTT confer the opposite phenotypes noted for eIF1A SI mutations. First, they reduce the rate of TC loading both *in vitro* and *in vivo*, as indicated by the Gcd[−] phenotype – Gcd[−] mutations overcome the translational repression of GCN4 mRNA by short uORFs. By reducing the rate of TC loading, they allow 40S subunits that translate the first uORF and resume scanning to bypass the subsequent uORFs 2–4 and reinitiate at the GCN4 ORF instead [46]. Second, the eIF1A SE substitutions increase initiation at UUG codons *in vivo* (Ssu[−] phenotype), and *in vitro* they stabilize eIF1A binding to the PIC at UUG codons and accelerate joining of the 60S to the 40S subunit [43, 44]. Together, these defects signify a shift from the open/P_{OUT} conformation to the closed/P_{IN} state, which diminishes the rate of TC loading to the open conformation and favors transition to the closed state at non-AUG codons during scanning. The deduced functions of the wild-type SE elements of promoting P_{OUT} and impeding P_{IN} were attributed [44] to the presence of the eIF1A CTT in the P site in a location that clashes with tRNA_i in the P/P conformation [41]. While the eIF1A CTT has not been directly visualized in PICs, hydroxyl radical cleavage of P-site residues in h30 directed by Cys residues in the yeast eIF1A CTT was suppressed in PICs reconstituted with AUG- versus AUC-containing mRNA, consistent with eviction of the eIF1A CTT from the P site on transition to the closed/P_{IN} conformation at AUG [31]. This rearrangement could be coupled with movement of

Figure 6. eIF1 and eIF1A Regulate the P_{IN} State of Met-tRNA_i Binding. (A) Overlay of eIF1 in the py48S complex (cyan) relative to that in a simpler PIC containing only eIF1 and eIF1A (salmon), revealing the deforming of eIF1 loops 1 and 2 and eIF1 displacement on the 40S platform to prevent a clash with tRNA_i bound in the P_{IN} state (image provided by José L. Llacer). (B) The *Tetrahymena* 40S–eIF1–eIF1A crystal structure reveals the eIF1A NTT bridging the 40S head and body by contacting S27e (rpS27a) and (S30e) rpS30, respectively. Scanning inhibitor element 1 (SI1) in the NTT is indicated, as is SI2, encompassing residues in the helical domain and its associated structured N and C strands. Also indicated are Ssu[−] substitutions (that suppress UUG initiation in Ssu[−] mutants) and a Gcd[−] substitution that impairs TC binding to the PIC [43, 44] (reproduced from [42]). (C) (Upper) The eIF1A-NTT assumes a defined conformation and interacts with the codon–anticodon duplex in the py48S PIC. (Lower) Specific contacts of the NTT and eIF1A-Trp70 with the AUG and +4 nucleotide in the mRNA, tRNA_i, or rRNA residues are indicated (reproduced from [20]). Abbreviations: eIF, eukaryotic initiation factor; NTT, N-terminal tail; PIC, preinitiation complex; TC, eIF2–GTP–Met-tRNA_i ternary complex.

the eIF1A CTT toward the eIF5-NTD on AUG recognition (Figure 3), detected by fluorescence resonance energy transfer analysis of reconstituted yeast PICs. This movement appears to be critical for P_i release from eIF2-GDP–P_i, as its rate and the rate of P_i release were similarly impaired by SE mutations [40].

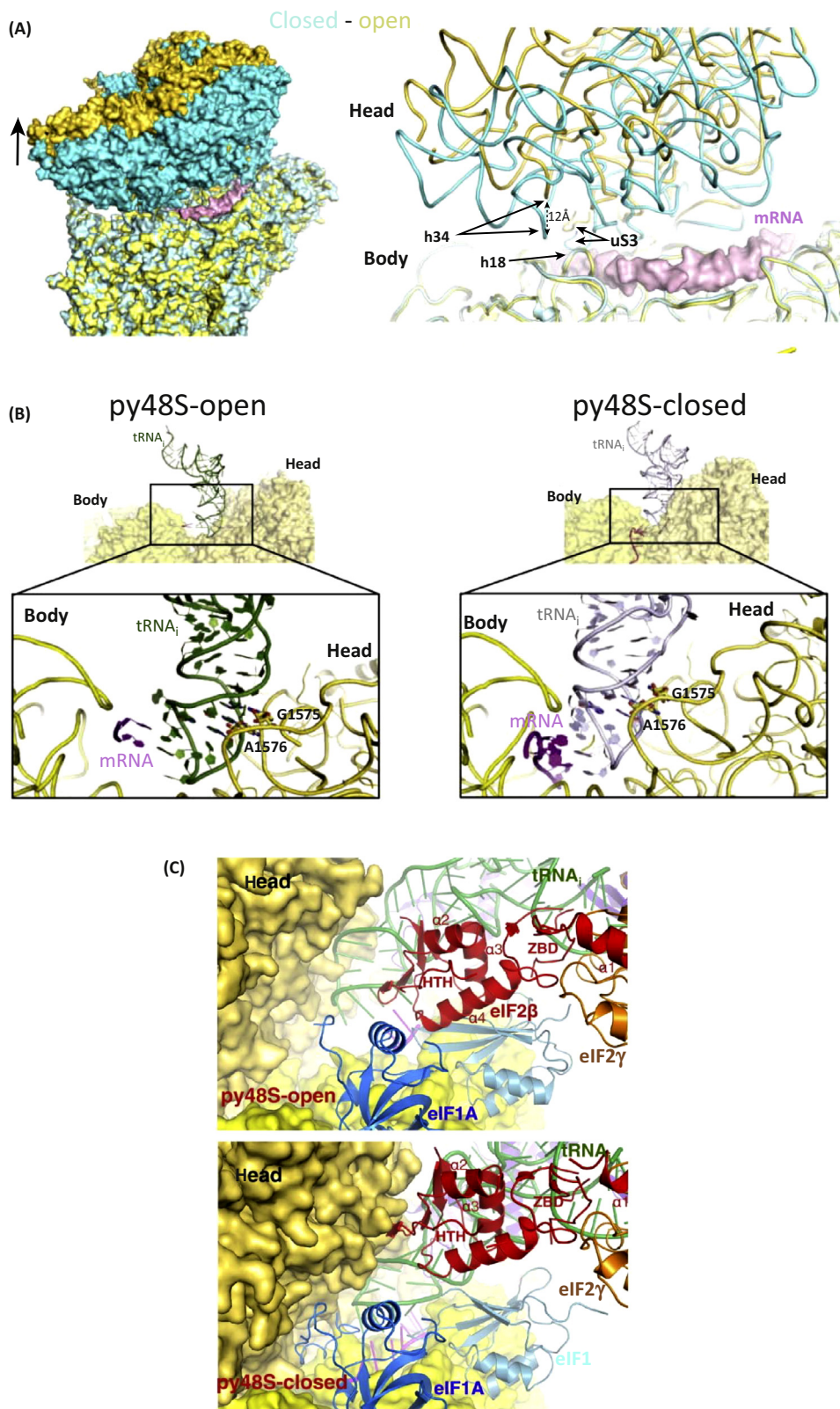
Thus, the unstructured tails of eIF1A have opposing roles during scanning. The NTT stabilizes the closed conformation and P_{IN} mode of tRNA_i binding by interacting with the codon–anticodon helix, to promote start codon recognition. The CTT, by contrast, enhances the open conformation and obstructs full accommodation of tRNA_i in the P site to favor continued scanning. The SE elements in the eIF1A-CTT also function in gating P_i release.

PIC Contacts with mRNA in the Closed/P_{IN} Complex

The mRNA path through the eukaryotic 48S PICs is similar to that observed in bacterial 70S elongation complexes except for the absence of a pronounced kink between the A and P sites, thought to help maintain reading frame during elongation. Absence of a kink in the PIC might facilitate slippage of the mRNA through the decoding center during base-by-base scanning [35]. mRNA residues both upstream and downstream of the AUG engage residues within 18S rRNA, ribosomal proteins, and initiation factors, which could be instrumental in producing pauses in scanning required for efficient start codon recognition or in stabilizing the closed/P_{IN} state. These include interactions of eIF2 α -D1 Arg residues with nucleotides 5' of the AUG [20] (Figure 4C), stacking of rRNA G1150 on the mRNA –1 nucleotide, and interactions of ribosomal proteins eS26 and eS28 with mRNA nucleotides further upstream of the AUG [20,35]. These last interactions could fix 5' UTR residues in the exit channel and help explain the requirement for a minimal 5' UTR length for efficient start codon recognition [47]. On the 3' side of the AUG codon, the key +4 nucleotide of the Kozak consensus stacks on Trp-70 of eIF1A, and the eIF1A NTT contacts the +4, +5, and +6 nucleotides in the A site [20] (Figure 6C).

The py48S-Open Complex Exhibits a Widened mRNA Channel, Open Latch, and Incomplete P Site Conducive to mRNA Recruitment and Scanning

An important structural feature of the mRNA entry channel is a noncovalent interaction between rRNA residues in h34 of the 40S head and h18 of the body, comprising a 'latch' thought to clamp mRNA into the entry channel. The first, relatively low-resolution cryo-EM structure of yeast 40S PICs harboring eIF1, eIF1A, or both, indicated an open latch in the 40S–eIF1–eIF1A PIC but a closed latch in the free 40S and 40S–eIF1A complex, consistent with an open, scanning conformation induced by eIFs 1 and 1A [29]. However, the latch is closed in crystal structures of the *Tetrahymena* [42] and mammalian [35] 40S–eIF1–eIF1A complexes, and in all other PIC structures obtained prior to the recent cryo-EM reconstruction of a yeast 48S PIC in an open conformation, dubbed py48S-open [21]. Py48S-open was assembled using mRNA with AUC versus AUG start codon, and WT eIF2 and tRNA_i instead of the tRNA_i-U31:A39 and eIF2 β -S264Y Sui⁺ variants employed previously to stabilize the closed/P_{IN} state. Another py48S-closed complex containing AUG mRNA was also resolved using WT eIF2, highly similar to the previous py48S except that most of the eIF2 β subunit was visible, as well as density for eIF3 subunits [21] (more about eIF3 below). Compared with py48S-closed, py48S-open exhibits upward movement of the head from the body, achieved by a 7–8 Å increase in the pitch of h28 that widens the entry channel and opens the latch (Figure 7A). Biochemical support for the widened entry channel of py48S-open came from enhanced sensitivity to hydroxyl radical cleavage of rRNA residues lining the entry channel of yeast PICs reconstituted with AUC- versus AUG-containing mRNAs [31]. As the head movement and latch opening were not observed in a py43S complex (lacking mRNA but containing TC and eIFs 1/1A) resolved in the same study, nor in the mammalian pm43S [24], both conformational changes might require mRNA. At any rate, it now appears that eIF1 and eIF1A (present in all of these PICs) are not



sufficient for latch opening. Compared with py48S-closed, there are many fewer contacts between the PIC and mRNA nucleotides 3' of the AUG of py48S-open, presumably reflecting its widened entry channel and open latch – properties that could facilitate mRNA attachment or scanning [21]. However, the closed-latch conformation of the m43S PIC bound to Dhx29 [24] [28], an RNA helicase that promotes scanning through structured 5' UTRs [93], might indicate that latch closure is required for processive scanning and that the open-latch conformation of py48S-open is more relevant to mRNA attachment.

Owing to upward head movement in py48S-open, the P site is incompletely formed, displaying canonical tRNA_i contacts with the 40S head, including G1575/A1576 with the ASL (Figure 5A, B), but lacking tRNA_i contacts with the 40S body observed in py48S-closed (Figure 7B). The widened P site results from lateral displacement of the head and associated tRNA_i ASL away from the 40S body by ~7 Å. The lack of contacts between the tRNA_i ASL and 40S body, and presumably less stable binding of TC to the py48S-open, might facilitate reiterative triplet sampling during scanning in the manner envisioned for the P_{OUT} state. Although the ASL is deep in the P site of py48S-open and base paired to the AUC codon, the tRNA_i exhibits a novel conformation (dubbed sP/I for 'scanning P/I'). Other features of py48S-open consistent with a scanning conformation include a disordered eIF1A NTT, absence of a clash between tRNA_i and eIF1 and lack of the attendant movement and distortion of eIF1 seen in py48S-closed, and absence of contacts between eIF2α-D1 residues and the –3 nucleotide of the mRNA [21]. These last contacts require a rotation of eIF2α-D1 to avoid a clash with the 40S body that occurs in the transition to the closed complex [21].

In summary, the widened entry channel and its lack of fixed contacts with mRNA, plus an incompletely formed P site that is missing certain contacts needed to lock tRNA_i into a stable P_{IN} state, should render the py48S-open complex conducive to scanning.

elF2β Exhibits Contacts with eIF1, eIF1A, and the tRNA_i ASL Restricted to py48S-Open

In previous py48S [20] and pm43S [24] structures, only the N-terminal helix of elF2β was visualized, where it attaches to elF2γ. However, most of elF2β is visible in py48S-open and py48S-closed structures (excluding the unstructured NTT), and it interacts differently with PIC components in these two complexes. In py48S-open, the helix-turn-helix domain of elF2β binds to both tRNA_i (anchored to the 40S head) and eIFs 1 and 1A (bound to the 40S body), bridging the head and body. These interactions with eIFs 1 and 1A cannot occur in py48S-closed owing to steric clashes, and elF2β interacts with the 40S head instead. The elF2β-tRNA_i interactions are also remodeled in the proposed transition from open to closed conformations of py48S (Figure 7C). Substitutions in elF2β or eIF1 that should perturb their interface in py48S-open confer increased initiation at both UUG codons (Sui⁺ phenotype) and the suboptimal AUG of eIF1 mRNA, consistent with enhanced transition to the closed state at poor initiation sites during scanning. elF2β substitutions that perturb its interface with tRNA_i in py48S-open confer the Gcd⁺ phenotype, indicating reduced TC recruitment to the open conformation, in addition to a Sui⁺ phenotype. These genetic data support the physiological importance of elF2β interactions with eIF1 and eIF1A in stabilizing specifically the open, scanning conformation of the PIC [21].

Figure 7. Comparison of Open and Closed Conformations of py48S. (A) Upward movement of the 40S head from the body in the py48S-open complex formed with AUC-containing mRNA (gold) versus the AUG complex py48S-closed (cyan) opens the mRNA entry channel latch and mRNA binding cleft. (B) The relative head–body movement shown in (A) eliminates contacts between the 40S head and Met-tRNA_i in py48S-open (left) versus py48S-closed (right). (C) elF2β interacts with eIF1 and eIF1A in py48S-open (top) but not in py48S-closed (bottom) (Panels A–C reproduced from [21]). elF, eukaryotic initiation factor.

TC is also remodeled in the open to closed transition. eIF2 α -D3 and eIF2 β both interact with eIF2 γ , and the eIF2 α -D3/ β / γ assembly moves as a unit relative to both eIF2 α -D1-D2 and tRNA_i between py48S-open and py48S-closed [21] (Figure 7C). Interactions of eIF2 α D1 and D2 with tRNA_i are also remodeled in this transition. By contrast, the interface between the GTP-binding pocket in eIF2 γ and the zinc-binding domain of eIF2 β [21], where most eIF2 β Sui⁺ substitutions reside [48], does not vary between the two conformations. Thus, there is no structural basis to support the possibility that remodeling of the interface between the eIF2 γ G-domain and eIF2 β zinc-binding domain enhances GTP hydrolysis by eIF2 in the transition from open to closed conformations. This is not surprising, however, since P_i release is more highly stimulated by AUG recognition than is GTP hydrolysis *per se* in yeast PICs [49]. The structural basis for the role of eIF1 dissociation in gating P_i release on start codon recognition is not currently understood.

These findings revealed that various contacts of eIF2 subunits with tRNA_i, eIF1, and eIF1A are remodeled in the transition from the open to closed conformation of the py48S PIC, and that eIF2 β -eIF1 interactions uniquely stabilize the open, scanning conformation.

Insights from Prokaryotic PICs

Recent cryo-EM analysis of bacterial (*Thermus thermophilus*) PICs containing IF1 and IF3—the functional orthologs of eIF1A and eIF1 – revealed parallels with eukaryotic PICs suggesting conservation of key aspects of initiation [50]. In prokaryotes, the purine-rich Shine–Dalgarno (SD) sequence just upstream of the start codon pairs with the 3' end of 16S rRNA in the small (30S) subunit to direct the PIC to the correct start codon, supplanting the scanning mechanism, although scanning appears to operate during reinitiation events on polycistronic mRNAs [51]. A subset of the observed 30S-IF1-IF3-mRNA PIC structures revealed a conformation similar to the yeast py48S-open, with upward displacement of the 30S head from the body that opens the latch on the mRNA entry channel and widens the P site, such that the (formylated) fMet-tRNA_i^{fMet} is not tightly locked-in. This open conformation should be conducive to PIC attachment to the mRNA. All other observed structures revealed the closed conformation, more similar to py48S-closed, and displayed different orientations of fMet-tRNA_i^{fMet} in the P site consistent with a progression toward full accommodation, involving rotation of the 30S head and compression of h28, as seen in eukaryotic PICs. Interestingly, these conformational changes in fMet-tRNA_i^{fMet} are accompanied by progressively larger alterations in the conformation and position of the CTD of IF3, which binds on the platform in much the same position as eIF1 in eukaryotes, and like eIF1, must be distorted and repositioned to avoid a clash with fMet-tRNA_i^{fMet} when accommodated in the P site [50]. This clash likely contributes to IF3's known function in discriminating against noncognate tRNAs or start codons (see [52]). In fact, it was shown that mammalian eIF1 and bacterial IF3-CTD can each bind to the same regions of the small subunit, and discriminate against initiation complexes with codon–anticodon mismatches, in the heterologous *in vitro* systems [34]. Interestingly, however, the IF3-CTD exhibits a much larger displacement from the P site (of 25 Å) on full accommodation [50], than observed thus far for yeast eIF1.

The remodeling of eIF1/IF3-CTD during accommodation of tRNA_i noted above was also observed for the archaeal counterpart, alF1, in a *Pyrococcus abyssi* PIC displaying a P_{IN} conformation (dubbed IC1) [53], thus suggesting a universal mechanism for promoting initiation accuracy in all three kingdoms of life. However, the archaeal IC1 differs substantially from the yeast py48S-closed [21] in displaying contacts between h44 in the 30S subunit and the G-domain of alF2 γ . To accommodate base pairing with the AUG codon, this 30S-alF2 γ interaction imposes a bend in tRNA_i and attendant remodeling of its contacts with alF2 subunits compared to those seen in free tRNA_i. It was proposed that the energetic penalty for this structural constraint demands a perfect codon–anticodon duplex and thereby enforces

stringent selection of AUG as start codon [53]. A distinct PIC conformation, IC0, also exhibits the 30S/G-domain contacts, plus additional 30S contacts involving eIF2 γ -II and eIF2 α -III, but the ASL of the tRNA i is swung out of the P-site in a ‘P_{REMOTE}’ conformation. The aTC conformation in IC0 is highly similar to that of free aTC, and thus unconstrained. The P_{REMOTE} conformation is proposed to exist during scanning, with transition to IC1-P_{IN} occurring on AUG recognition. Noting that codon–anticodon pairing already exists in the yeast py48S-open complex [21], and citing DHRC evidence for h44 contacts by the eIF2 γ G-domain in yeast 48S PICs [54], it was envisioned that the P_{REMOTE} conformation might also exist in scanning eukaryotic PICs. Interestingly, in IC0-P_{REMOTE}, the NTT of eIF1 approaches the GTP-binding pocket of the eIF2 γ G-domain and eIF1 appears to be more tightly bound to the platform than in IC1-P_{IN}, consistent with its release from the PIC on AUG recognition. If eIF1-eIF2 γ contact occurred in scanning eukaryotic PICs, it could underlie the gatekeeper function of eIF1 in blocking P_i release from eIF2-GDP-P_i at non-AUG codons [53]. However, the eIF1-eIF2 β interface (Figure 7C) shown to stabilize the scanning yeast PIC [21] is not evident in IC0-P_{REMOTE}. Moreover, eIF2 α -D1 does not occupy the E site in either IC0 or IC1, probably reflecting the presence of the SD/anti-SD duplex in the exit channel [53], in sharp contrast to py48S complexes where eIF2 α -D1’s contacts with the mRNA –3 nucleotide (Figure 4C) likely influence start codon selection [20].

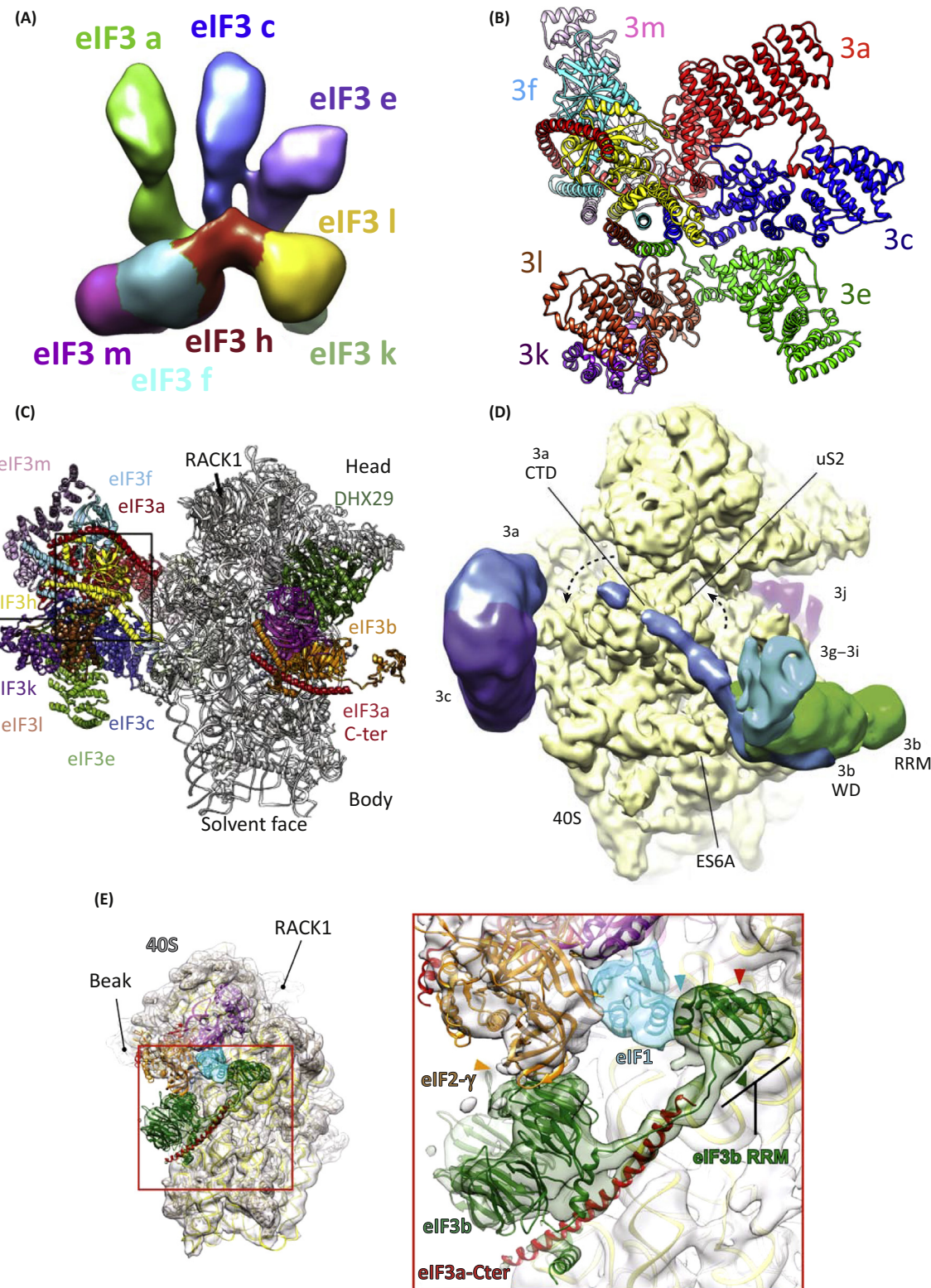
These recent structures of bacterial and archaeal PICs indicate that remodeling of the interaction of eIF1/eIF1/IF3-CTD with the small subunit to avoid a clash with tRNA i ^{Met} is a conserved feature that likely contributes to rejection of non-AUG initiation codons in all three kingdoms of life. Other conserved features include movement of the 40S head to constrict the mRNA binding cleft on start codon recognition, the occurrence of nonaccommodated conformations of tRNA i that appear conducive to scanning, and distortion of the tRNA i molecule on start codon recognition in a manner that could help restrict initiation to AUG codons. There are, however, both quantitative and qualitative differences in the conformational rearrangements of the PIC observed in the three different systems.

Structure of eIF3

Because of its subunit complexity and absence in archaea, and the conformational flexibility of linkers connecting its globular subdomains, the complete structure of eIF3 has not yet been determined. However, substantial progress has been made toward this goal, and the interaction of its globular subdomains with the PIC was recently illuminated.

The subunit interaction map of the yeast eIF3 complex (Figure 2) was constructed by mapping binary interactions between its six subunits, and identifying stable native subcomplexes formed with truncated versus full-length subunits (reviewed in [5,55]). Thus, the 3i and 3g subunits form a subcomplex via the 3g-NTD, and the N-terminal half of 3a interacts with 3c to form a second subcomplex. The 3b subunit bridges these two subcomplexes, binding to 3i and 3g with its CTD and to a C-terminal segment of 3a (the Hcr1-like domain or HLD) through its N-terminal RNA recognition motif (RRM), and both the 3b-RRM and 3a-HLD bind to the NTD of 3j. Analysis of native 40S association by different eIF3 subcomplexes [56,57], and identification of interactions of individual eIF3 subunits with segments of rRNA or 40S proteins (summarized in Figure 2), revealed interactions of different yeast eIF3 subunits with the entry and exit channels for mRNA on the solvent-exposed face of the 40S subunit. This supported the proposal that eIF3 physically extends the entry and exit channels, based on crosslinking of eIF3 subunits to mRNA at the exit channel, and eIF3 protection of rRNA at the entry channel from chemical or enzymatic modification/cleavage in reconstituted mammalian PICs [58].

High-resolution crystal or solution structures have been determined for multiple domains of yeast eIF3 subunits, or their mammalian orthologs, and of various subcomplexes of eIF3 subunits/



domains. These include the yeast [59] and human 3b-RRM [60] and its subcomplex with the N-terminal segment of human 3j [61], the RRM of human 3g [62], the nine-bladed β -propeller domain of 3b [63,64], and the seven-bladed β -propeller of yeast 3i bound to the C-terminal helix of 3b [65] and the 3g-NTD [64]. The proteasome-COP9-initiation factor (PCI) domains in human 3k [66] and the yeast 3a-NTD [59], and the heterodimer of the 3a/3c PCI domains [64] have also been solved. While yelF3 contains only two PCI subunits (3a/3c), the 13-subunit melF3 contains six, and also two subunits not present in yeast with the MPN motif, which also participates in protein–protein interactions. Interestingly, the 26S proteasome lid and COP9 signalosome exhibit the same 6-PCI/2-MPN subunit stoichiometry and provided structural models for the octameric core of melF3. The high-resolution structures of individual eIF3 subunits/subcomplexes were invaluable in achieving cryo-EM reconstructions of both mammalian and yeast PICs containing eIF3.

Structural analysis of melF3 advanced substantially with a cryo-EM reconstruction of the human factor, revealing a five-lobed structure with appendages reminiscent of a head, two arms, and legs. A model of melF3 docked on the 40S subunit, generated using reconstructions of the hepatitis C virus internal ribosome entry site (HCV IRES) bound separately to the 40S or melF3 [67], revealed most of the density on the solvent-exposed surface of the 40S near the exit channel. This agreed with a previous 48 Å negative stain-EM reconstruction of native 43S PICs [68], crosslinking of the 3a and 3d subunits to mRNA 5' UTR residues in mammalian 48S PICs [58], and interactions of yelF3 subunits with 40S components (Figure 2). Mass spectrometry of melF3 subcomplexes dissociated from the holocomplex in high salt revealed a yeast-like 3a/3b/3c/3g/3i subcomplex, but also separate complexes containing the PCI subunits 3c/3e/3k/3l/3m and MPN subunits 3f/3h [69]. An octameric complex of all mammalian PCI/MPN subunits (3a/3c/3e/3k/3l/3m and 3f/3h) was reconstituted from recombinant subunits; and both negative-stain EM [70] and cryo-EM analysis [71] of the resulting complex revealed essentially the same five-lobed structure seen for native melF3, even though half of the total mass was lacking in the reconstituted complex. This implied that the other five melF3 subunits (3b/3i/3g/3d/3j) are highly mobile. The locations within the five-lobed structure of the N-termini of all but one of the six PCI subunits (3c), of the MPN subunits (3f/3h), and noncore subunits 3d and 3j were assigned by EM analysis of complexes reconstituted with N-terminally tagged subunits (Figure 8A). This analysis, combined with a comparison to the cryo-EM model of the proteasome lid, suggested that the five appendages of eIF3 are composed of the PCI domains of subunits 3a (left arm), 3c (head), 3e (right arm), 3l/3k (right leg), and 3m (left leg), with the MPN subunits 3f/3h occupying the torso at the junction of the two legs. This model (Figure 8A) is consistent with the eIF3 subcomplexes detected by mass spectrometry [69].

Although the reconstituted PCI/MPN octamer could bind to the 40S subunit, the remaining eIF3 subunits were required to form a functional PIC with the HCV IRES [71]. Independent reconstitution experiments showed that a subcomplex of PCI subunits 3a/3c/3e, the MPN subunits 3n/3l, and the 3b subunit comprise a minimal complex that functions comparably to melF3

Figure 8. eIF3 Architecture and Location within the PIC. (A) Cryo-EM reconstruction of the octamer reconstituted from mammalian PCI/MPN subunits and the assignment of its appendages by imaging complexes assembled with tagged subunits (reproduced from [71]). (B) Polyalanine-level model of the eIF3 PCI/MPN octamer visualized in the m43S PIC, showing the seven-helix bundle formed by subunits h, c, e, l, f, and k (image provided by Yaser Hashem). (C) Location of eIF3 subunits in the m43S PIC, with the PCI/MPN octamer bound below the platform near the mRNA exit channel via 40S contacts with 3a and 3c; and peripheral domains bound near the mRNA entry channel, including the β -propellers of 3b and 3i, juxtaposed and linked together by a C-terminal helix of 3b, the 3b N-terminal RRM, and a helical segment attributed to the 3a-CTD (reproduced from [28]). (D) Location of yeast eIF3 domains in a cryo-EM reconstruction of a 40S–eIF1–eIF1A–eIF3 complex. The 3a/3c PCI heterodimer is bound below the mRNA exit channel (broken arrow). A subcomplex of the 3b β -propeller, 3b RRM, 3i β -propeller (presumably complexed with the 3g-NTD), and a segment of the 3a-CTD is bound below the entry channel (broken arrow), similar to the locations of the homologous domains in the m43S PIC in (C) (reproduced from [81]). (E) Proposed interaction of the 3b β -propeller and 3b RRM with eIF2 γ and eIF1, respectively, on the interface surface of the 40S subunit, implying relocation of 3b from its position on the solvent-exposed face of the 40S–eIF1–eIF1A–eIF3 complex shown in D (reproduced from [91]). Abbreviations: Cryo-EM, electron cryomicroscopy; CTD, C-terminal domain; eIF, eukaryotic initiation factor; NTD, N-terminal domain; PCI, proteasome-COP9-initiation factor; PIC, preinitiation complex; RRM, RNA recognition motif.

holocomplex in 48S PIC assembly on β -globin mRNA [72]. This minimal core presumably contained the two arms, head, and body of the PCI/MPN octamer connected to the more mobile 3b subunit. In *Neurospora crassa*, the 3e/3h/3k/3l subunits are not essential for viability [73], and are clustered together in the right arm (3e), right leg (3k/3l), and part of the torso (3h) of the melF3 model (Figure 8A). Indeed, a subcomplex purified from a translationally compromised, *N. crassa* 3h deletion mutant lacks all three dispensable PCI subunits plus 3d and exhibits a human-like eIF3 structure but lacking the right arm and leg [74]. As discussed next, analysis of the m43S PIC suggests that these dispensable subunits are not present at the 40S interface and instead project out into solution where they presumably mediate nonessential interactions with mRNA or signaling molecules. Thus, a combination of biochemical and structural analyses has identified a stable octamer of PCI/MPN-domain subunits in melF3, of which only two PCI subunits exist in yelF3 (3a/3c), plus a functionally important 3g/3i domain that is connected to the PCI/MPN domain by the 3b subunit.

Position of melF3 in the Mammalian 43S PIC

The PCI/MPN octamer of melF3 was visualized in the cryo-EM reconstructions of the m43S PIC bound to Dhx29, first at 11.6 Å [24] and later at ~6 Å [28] (Figure 8B,C). The head and left arm, composed of 3c and 3a [71], contact ribosomal proteins Rps13/S15 and Rps27/S27e, and Rps3A/S1e and Rps26/S26e, respectively, on the solvent face of the 40S near the exit channel (Figure 8C). This position of 3a fits with its crosslinking to mRNA 5' UTR residues –14/–17 (relative to AUG) in mammalian 48S PICs [58]. Subunits 3a/3c interact with 3e to comprise the rigid PCI core of the complex. Consistent with the protection of h16 residues from chemical or enzymatic cleavage by melF3 in reconstituted 40S–eIF3–poly(U) complexes [58], additional density at the 40S entry channel was assigned to the β -propeller of 3b, and proximal, low-resolution density projecting toward the 40S beak was tentatively assigned as the 3b-RRM (Figure 8C). Other low-resolution density connected to the 3b β -propeller was attributed to the seven-bladed β -propeller of eIF3i, known to interact with the CTT of 3b (Figure 2), which appears to emanate from the eIF3b β -propeller [28] (Figure 8C). An extended helical density spanning the 3b β -propeller was assigned to a segment of the 3a-CTD [28] (Figure 8C), although known 3b/3a-CTD interactions in yelF3 (Figure 2) and mammals [75] involve the 3b RRM.

It is known that melF3 interacts with eIF4G, bridging interaction between eIF3 in the 43S PIC and the eIF4F-mRNP [2]. Integrating information about melF3 subunits in the PCI/MPN core that interact with eIF4G (3e/3c/3d) [76,77] and DHRC data identifying eIF4G middle domain (eIF4Gm) interactions with expansion segment 6 near the bottom of the 40S [78], the eIF4Gm and adjacent eIF3 binding domain were tentatively positioned on the solvent-exposed face below the platform in the vicinity of the exit channel [28]. However, eIF4G is large enough to also interact with the mRNA entry channel [79], where it could position eIF4A for unwinding mRNA secondary structures and eIF4E for its recently proposed function of feeding the capped 5' end of the mRNA into the entry channel at the stage of PIC attachment to mRNA [80].

In summary, the PCI/MPN octamer of melF3 binds to the solvent-exposed surface of the 40S subunit near the mRNA exit channel, whereas the 3b-3i-3g subdomain is located near the entry channel, in accordance with known melF3 interactions with mRNA and its role in mRNA recruitment by the PIC.

Position of yelF3 in a 40S–eIF1–eIF1A–eIF3 PIC

Interaction of the six-subunit yelF3 complex with the 40S subunit was revealed in a cryo-EM reconstruction of a 40S–eIF1–eIF1A–eIF3 complex, stabilized by crosslinking, at ~6.5 Å resolution [81] (Figure 8D). Interpreting the eIF3 densities was aided by prior crosslinking-mass

spectrometry, which identified 155 linkages between yelF3 subunits and 40S ribosomal proteins, and integrative modeling [64]. The best-defined aspects include the 3a/3c PCI heterodimer near the mRNA exit channel, similar to its location in the m43S PIC except that the C-terminal portion of the 3a PCI domain occupies the approximate position of mammalian 3f/3h, absent in yeast. This location of the yeast PCI domains is consistent with physical interaction of yeast 3a-NTD with uS2/Rps0 [82] and functional interaction of the 3a-NTD with mRNA sequences upstream of the GCN4 uORF1 expected to reside in the exit channel during reinitiation events [83,84]. The other well-defined density in the 40S–eIF1–eIF1A–eIF3 complex corresponds to the 3b β -propeller bound on the solvent side below the entry channel in contact with uS4/Rps9, similar to its location in the m43S PIC [28,63]. Two regions of weakly ordered density attached to the eIF3b β -propeller were assigned to the eIF3b RRM and the trimeric subcomplex composed of the 3i β -propeller, 3g-NTD, and 3b C-terminal helix [64,65], which project into solution in different directions, with the RRM oriented toward the 40S beak. Because the presumptive 3b-CTD/3i/3g-NTD subcomplex does not contact the 40S subunit, this structure does not rationalize contributions of the 3i/3g subcomplex to 40S binding by eIF3 *in vivo*, deduced from analysis of a 3i mutation (*tif34-DD/KK*) [65] nor does it account for other genetic findings on *tif34-DD/KK* and *tif34-Q258R* [65] that implicate the 3i/3g module in scanning and AUG recognition *in vivo*. However, given that 3g can bind to isolated uS3/Rps3 and uS10/Rps20 [62], which are located at (uS3) or near (uS10) the mRNA entry channel, the 3i/3g subcomplex might interact dynamically with the 40S entry channel to promote eIF3–40S association and modulate scanning *in vivo*.

The 3b RRM has also been shown to promote 40S binding by yelF3 and enhance AUG selection during scanning *in vivo*, with both functions depending on its direct interaction with the NTD of eIF3j [60,61,85]. A 3j point mutation that disrupts interaction with the 3b-RRM dramatically increases leaky scanning [61], indicating that the 3b connection to both the 3j-NTD and 3i/3g module, involving opposite ends of 3b, enhances AUG selection by the scanning PIC. The CTD of mammalian 3j can bind directly to the 40S mRNA entry channel in a manner anticooperative with eIF1A binding in the A site [86]. Based on these findings, and crosslinking mass spectrometry data [64], density in the yeast 40S–eIF1–eIF1A–eIF3 complex located in the 40S entry channel abutting eIF1A was assigned to 3j (Figure 8D), although its known connection with the presumptive 3b-RRM was not observed and might be flexible or transient [81].

In the yeast 40S–eIF1–eIF1A–eIF3 complex, the 3b β -propeller is also connected to an elongated density, assigned to the 3a/CTD, which extends back across the 40S subunit toward the 3a/3c PCI heterodimer and contacts uS2/Rps0 on the solvent-exposed face of the 40S subunit [81] (Figure 8D). The same linkage involving the 3a-CTD was inferred by similar assignments of the 3a/3c PCI heterodimer and 3b β -propeller in both the py48S-closed complex [21] and m43S PIC (Figure 8C), and supported by the known role of the yeast 3a-CTD in connecting the 3c/3a heterodimer to the 3b/3g/3i subunits [56], of promoting 40S binding of eIF3 *in vivo* [57], and its ability to bind *in vitro* to isolated uS3/Rps3, uS5/Rps2 [87], and an 18S rRNA subdomain of h16-h18 [57] (all constituents of the entry channel; Figure 2). The proximity of yelF3 subunits to both the mRNA exit and entry channels of the 40S subunit is consistent with the critical importance of eIF3 in attachment of 43S PICs to mRNA both *in vivo* [88] and in a yeast reconstituted system [89]. Point mutations in the 3a-CTD that destabilize the 3a-CTD/3b-RRM/3j-NTD subassembly impair formation of native 48S PICs *in vivo* and appear to reduce the processivity of scanning and efficiency of start codon recognition [87]. These mutations in 3a, and the 3i mutation *tif34-DD/KK*, reduce the rate of native mRNA recruitment *in vitro*, implicating eIF3 in PIC interactions with mRNA at the entry channel. The N-terminal PCI domain of 3a was also shown to mediate stabilizing interactions with mRNA at the exit channel *in vitro* [90].

In summary, the structural findings reveal that the 3a-3c PCI heterodimer and 3b-3i-3g module of eIF3 bind near the exit and entry channel opening on the solvent-exposed surface of the 40S subunit, much as observed for mIF3, rationalizing the effects of certain eIF3 mutations on mRNA recruitment, scanning, and accurate start codon recognition *in vivo*.

Communication of eIF3 Subunits with the Decoding Center in Yeast PICs

The connections identified in the yeast MFC (Figure 2) led to the prediction that the 3c-NTD and 3a-CTD segments project into the subunit interface side of the 40S subunit and interact with eIF1, eIF2 β -NTT, and eIF5-CTD in the decoding center [7,8]. Consistent with this, crosslinking mass spectrometry data indicates interaction of the N-terminal segment of eIF3c with eIF1 bound to the 40S platform [64]. Moreover, a globular density was found in contact with eIF1 in the py48S-closed complex and tentatively assigned to the eIF3c-NTD, with connections to the 3c PCI domain via flexible linkers and a helical bundle [21]. This density also contacts helical segments assigned to the 3a-CTD, which was envisioned to project across the subunit-interface surface of the 40S after spanning the solvent-exposed face of the 40S from its origin at the 3a PCI domain, effectively encircling the PIC. Density interpreted as the 3i β -propeller in association with the 3g-NTD and 3b-CTD was found unexpectedly on the subunit interface beneath the eIF2 γ subunit of TC in py-48S-closed [21]. However, it was recently suggested that the drumlike density attributed to the 3i β -propeller is actually the larger β -propeller of 3b, and that the density in contact with eIF1 is the 3b-RRM rather than 3c-NTD [91] (Figure 8E). These reassessments are likely to be correct (J. Llacer, personal communication). The proposed locations of the 3b β -propeller and RRM in py48S-closed [91] (Figure 8E) imply a dramatic relocalization of the 3b/3i/3g module from its position on the solvent-exposed surface near the entry channel seen in the yeast 40S-eIF1-eIF3 [81] (Figure 8D) and mammalian pm43S [28] complexes (Figure 8C) that enables direct communication of the 3b β -propeller with eIF2 γ and the 3b RRM with eIF1 in the decoding center. While ample evidence exists for physical and functional interaction of the 3c-NTD with eIF1 (Figure 2) [11,64], interaction of the 3b-RRM with eIF1 requires independent confirmation. The ability of eIF3 to effectively encircle the 40S subunit, interacting with the entry and exit channels of the 40S subunit, and with all of the other initiation factors bound in the decoding center [21], rationalizes its ability to stimulate nearly every step of the initiation pathway [5,90].

Concluding Remarks

The recent high-resolution structures of PICs harboring different combinations of factors and ligands have provided a wealth of information about the mechanism of start codon recognition at atomic-level resolution, and identified certain aspects of the process that are conserved among all three kingdoms of life. The eukaryotic PIC structures have revealed distinct open or closed conformations of the 40S that seem conducive to mRNA attachment or scanning versus AUG selection, respectively. The open conformation exhibits a widened mRNA binding cleft and P site and less extensive interactions with mRNA and tRNA_i compared with the closed state; and the two states are interconvertible through movements of the head relative to the body of the 40S subunit. A more dramatic displacement of tRNA_i from the P site was observed in an archaeal PIC, which also seems suitable for scanning. Several structures indicated that full accommodation of tRNA_i in the P site requires distortion and movement of eIF1 on the 40S platform to avoid a clash between eIF1 and tRNA_i, thus helping to explain eIF1's role in limiting the open-to-closed transition to cognate (AUG) start codons, and suggesting how AUG recognition ultimately triggers eIF1 dissociation from the 40S. Displacement of eIF1's counterparts in bacteria (IF3-CTD) and archaea (aIF1) on tRNA_i accommodation was also seen, indicating a universal mechanism for achieving initiation accuracy. The observed interaction of the eIF1A-NTT with the codon–anticodon duplex rationalizes its role in preferentially promoting the closed/P_{IN} conformation, which is critical for utilizing poor initiation sites *in vivo*. The

Outstanding Questions

What is the functional significance of relocalization of the 3b/3i/3g module of eIF3 from the solvent side to the interface surface of the 40S, and its interactions with eIF2 γ and eIF1 in the decoding center?

Are the P_{REMOTE} orientations of TC and eIF1 contacts with the aIF2 γ G domain seen in the archaeal ICo PIC relevant to scanning and gated P_i release in eukaryotes?

What are the locations and interaction partners in the PIC of the NTD and CTD of eIF5 at different stages of initiation?

What is the structural basis for the role of the SE elements of the eIF1A-CTT in gating P_i release?

What are the locations of the eIF4F components and PABP in the scanning PIC?

Is eIF4E positioned in the PIC to feed the capped mRNA 5' end into the entry channel pore?

functions of all three subunits of eIF2 in contacting the tRNA_i within TC and determining tRNA_i conformation and orientation in the P site in different states were illuminated, as well as direct contacts of eIF2 α with the sequences surrounding the AUG codon that influence initiation frequency. Previously unsuspected interactions of eIF2 β with eIF1 and eIF1A were shown to stabilize exclusively the open conformation and promote continued scanning at poor initiation sites. Finally, the structures of the PCI/MPN core of eIF3, and the corresponding PCI heterodimer of eIF3, were elucidated and shown to attach near the exit channel of the 40S subunit, consistent with genetic and biochemical evidence implicating the eIF3a PCI domain in 40S-mRNA interactions at this location. The structure of the eIF3-3b/3i/3g domain was also resolved, and localized near the 40S entry channel in several structures but relocated to the decoding center in others. It is striking that eIF3 essentially encircles the PIC with its different subunits in proximity to all of the key functional sites of the 40S subunit, thus helping to explain its multifunctionality.

Additional work is required to evaluate the functional significance of the dramatic relocalization of the 3b/3i/3g module and its interactions with eIF2 γ and eIF1 in the decoding center, and the relative importance of eIF1 interactions with the 3b-RRM versus the 3c-NTD. It is also important to determine whether the open conformation of the py48S-open complex is relevant only to mRNA attachment, and whether a distinct P_{OUT} state exists during scanning with a closed-latch conformation to insure processivity. It is crucial to understand the structural basis of gated P_i release from eIF2-GDP-P_i, which irreversibly commits the PIC to a start codon, and whether it involves interaction of eIF1 with the GTP-binding pocket of eIF2 γ in the manner observed in archaeal IC0 PIC, as well as the role of the eIF1A-CTT SE elements in this crucial reaction. The molecular basis of the eIF5 NTD's functions in stabilizing the closed/P_{IN} state and triggering P_i release [92], in addition to its role as the GAP for eIF2, should be explored, as well as the alternative interactions of the eIF5-CTD with the eIF1A-NTT, eIF1, and eIF2 β -NTT thought to occur at different stages of initiation to regulate eIF1 dissociation (Figure 3). Finally, there is a dearth of structural information concerning the locations and interactions of the eIF4 factors within the PIC. The recent proposal that a chain of interactions between eIF3, eIF4G, and eIF4E position eIF4E at the entry channel to facilitate feeding of the mRNA 5' end into the pore [80] requires confirmation from structural analysis, and determining the locations of eIF4A and eIF4B within the PIC should illuminate their functions in stimulating mRNA attachment and scanning through structured 5' UTRs [3] (see Outstanding Questions).

Acknowledgments

The author is grateful to Tanweer Hussain, Jose L. Llacer, and Yaser Hashem for critical comments on the manuscript, communicating results prior to publication, and providing images employed in the figures.

References

1. Hinnebusch, A.G. *et al.* (2007) Mechanism of translation initiation in the yeast *Saccharomyces cerevisiae*. In *Translational Control in Biology and Medicine* (Mathews, M., ed.), pp. 225–268, Cold Spring Harbor Laboratory Press
2. Jackson, R.J. *et al.* (2010) The mechanism of eukaryotic translation initiation and principles of its regulation. *Nat. Rev. Mol. Cell Biol.* 11, 113–127
3. Hinnebusch, A.G. (2011) Molecular mechanism of scanning and start codon selection in eukaryotes. *Microbiol. Mol. Biol. Rev.* 75, 434–467
4. Hinnebusch, A.G. (2014) The scanning mechanism of eukaryotic translation initiation. *Annu. Rev. Biochem.* 83, 779–812
5. Valasek, L.S. (2012) 'Ribozoomin' – translation initiation from the perspective of the ribosome-bound eukaryotic initiation factors (eIFs). *Curr. Protein Pept. Sci.* 13, 305–330
6. Phan, L. *et al.* (1998) Identification of a translation initiation factor 3 (eIF3) core complex, conserved in yeast and mammals, that interacts with eIF5. *Mol. Cell Biol.* 18, 4935–4946
7. Asano, K. *et al.* (2000) A multifactor complex of eukaryotic initiation factors eIF1, eIF2, eIF3, eIF5, and initiator tRNA^{Met} is an important translation initiation intermediate *in vivo*. *Genes Dev.* 14, 2534–2546
8. Valášek, L. *et al.* (2002) Direct eIF2-eIF3 contact in the multifactor complex is important for translation initiation *in vivo*. *EMBO J.* 21, 5886–5898
9. Singh, C.R. *et al.* (2004) Efficient incorporation of eukaryotic initiation factor 1 into the multifactor complex is critical for formation of functional ribosomal preinitiation complexes *in vivo*. *J. Biol. Chem.* 279, 31910–31920
10. Sokabe, M. *et al.* (2012) The human translation initiation multifactor complex promotes methionyl-tRNA_i binding to the 40S ribosomal subunit. *Nucleic Acids Res.* 40, 905–913
11. Valášek, L. *et al.* (2004) Interactions of eukaryotic translation initiation factor 3 (eIF3) subunit NIP1/c with eIF1 and eIF5 promote preinitiation complex assembly and regulate start codon selection. *Mol. Cell Biol.* 24, 9437–9455

12. Karaskova, M. *et al.* (2012) Functional characterization of the role of the N-terminal domain of the c/Nip1 subunit of eukaryotic initiation factor 3 (eIF3) in AUG recognition. *J. Biol. Chem.* 287, 28420–28434
13. Luna, R.E. *et al.* (2012) The C-terminal domain of eukaryotic initiation factor 5 promotes start codon recognition by its dynamic interplay with eIF1 and eIF2beta. *Cell Rep.* 1, 689–702
14. Luna, R.E. *et al.* (2013) The interaction between eukaryotic initiation factor 1A and eIF5 retains eIF1 within scanning preinitiation complexes. *Biochemistry* 52, 9510–9518
15. Sokabe, M. *et al.* (2006) Structure of archaeal translational initiation factor 2 betagamma-GDP reveals significant conformational change of the beta-subunit and switch 1 region. *Proc. Natl. Acad. Sci. U. S. A.* 103, 13016–13021
16. Yatime, L. *et al.* (2007) Structure of an archaeal heterotrimeric initiation factor 2 reveals a nucleotide state between the GTP and the GDP states. *Proc. Natl. Acad. Sci. U. S. A.* 104, 18445–18450
17. Stolboushkin, E. (2008) Crystal structure of the intact archaeal translation initiation factor 2 demonstrates very high conformational flexibility in the alpha- and beta-subunits. *J. Mol. Biol.* 382, 680–691
18. Schmitt, E. *et al.* (2010) Eukaryotic and archaeal translation initiation factor 2: a heterotrimeric tRNA carrier. *FEBS Lett.* 584, 405–412
19. Schmitt, E. *et al.* (2012) Structure of the ternary initiation complex eIF2-GDPNP-methionylated initiator tRNA. *Nat. Struct. Mol. Biol.* 19, 450–454
20. Hussain, T. *et al.* (2014) Structural changes enable start codon recognition by the eukaryotic translation initiation complex. *Cell* 159, 597–607
21. Llacer, J.L. *et al.* (2015) Conformational differences between open and closed states of the eukaryotic translation initiation complex. *Mol. Cell* 59, 399–412
22. Acker, M.G. *et al.* (2007) Reconstitution of yeast translation initiation. *Methods Enzymol.* 430, 111–145
23. Dong, J. *et al.* (2014) Conserved residues in yeast initiator tRNA calibrate initiation accuracy by regulating preinitiation complex stability at the start codon. *Genes Dev.* 28, 502–520
24. Hashem, Y. *et al.* (2013) Structure of the mammalian ribosomal 43S preinitiation complex bound to the scanning factor DHX29. *Cell* 153, 1108–1119
25. Sharifulin, D. *et al.* (2013) Ribosomal protein S5e is implicated in translation initiation through its interaction with the N-terminal domain of initiation factor eIF2alpha. *ChemBioChem* 14, 2136–2143
26. Visweswarah, J. (2015) The beta-hairpin of 40S exit channel protein Rps5/uS7 promotes efficient and accurate translation initiation *in vivo*. *Elife* 4, e07939
27. Pisarev, A.V. *et al.* (2006) Specific functional interactions of nucleotides at key –3 and +4 positions flanking the initiation codon with components of the mammalian 48S translation initiation complex. *Genes Dev.* 20, 624–636
28. des Georges, A. *et al.* (2015) Structure of mammalian eIF3 in the context of the 43S preinitiation complex. *Nature* 525, 491–495
29. Passmore, L.A. *et al.* (2007) The eukaryotic translation initiation factors eIF1 and eIF1A induce an open conformation of the 40S ribosome. *Mol. Cell* 26, 41–50
30. Koltz, S.E. *et al.* (2009) Kinetic and thermodynamic analysis of the role of start codon/anticodon base pairing during eukaryotic translation initiation. *RNA* 15, 138–152
31. Zhang, F. *et al.* (2015) Conformational changes in the P site and mRNA entry channel evoked by AUG recognition in yeast translation preinitiation complexes. *Nucleic Acids Res.* 43, 2293–2312
32. Kapp, L.D. *et al.* (2006) Yeast initiator tRNA identity elements cooperate to influence multiple steps of translation initiation. *RNA* 12, 751–764
33. Drabkin, H.J. *et al.* (1993) The role of nucleotides conserved in eukaryotic initiator methionine tRNAs in initiation of protein synthesis. *J. Biol. Chem.* 268, 25221–25228
34. Lomakin, I.B. *et al.* (2006) The fidelity of translation initiation: reciprocal activities of eIF1, IF3 and YciH. *EMBO J.* 25, 196–210
35. Lomakin, I.B. and Steitz, T.A. (2013) The initiation of mammalian protein synthesis and mRNA scanning mechanism. *Nature* 500, 307–311
36. Dong, J. *et al.* (2008) Genetic identification of yeast 18S rRNA residues required for efficient recruitment of initiator tRNA(Met) and AUG selection. *Genes Dev.* 22, 2242–2255
37. Rabl, J. *et al.* (2011) Crystal structure of the eukaryotic 40S ribosomal subunit in complex with initiation factor 1. *Science* 331, 730–736
38. Lomakin, I.B. *et al.* (2003) Position of eukaryotic initiation factor eIF1 on the 40S ribosomal subunit determined by directed hydroxyl radical probing. *Genes Dev.* 17, 2786–2797
39. Martin-Marcos, P. *et al.* (2013) β -Hairpin loop of eIF1 mediates 40S ribosome binding to regulate initiator tRNAMet recruitment and accuracy of AUG selection *in vivo*. *J. Biol. Chem.* 288, 27546–27562
40. Nanda, J.S. *et al.* (2013) Coordinated movements of eukaryotic translation initiation factors eIF1, eIF1A, and eIF5 trigger phosphate release from eIF2 in response to start codon recognition by the ribosomal preinitiation complex. *J. Biol. Chem.* 288, 5316–5329
41. Yu, Y. *et al.* (2009) Position of eukaryotic translation initiation factor eIF1A on the 40S ribosomal subunit mapped by directed hydroxyl radical probing. *Nucleic Acids Res.* 37, 5167–5182
42. Weisser, M. *et al.* (2013) The crystal structure of the eukaryotic 40S ribosomal subunit in complex with eIF1 and eIF1A. *Nat. Struct. Mol. Biol.* 20, 1015–1017
43. Fekete, C.A. *et al.* (2007) N-and C-terminal residues of eIF1A have opposing effects on the fidelity of start codon selection. *EMBO J.* 26, 1602–1614
44. Saini, A.K. *et al.* (2010) Regulatory elements in eIF1A control the fidelity of start codon selection by modulating tRNA(i)(Met) binding to the ribosome. *Genes Dev.* 24, 97–110
45. Martin-Marcos, P. (2011) Functional elements in initiation factors 1, 1A, and 2beta discriminate against poor AUG context and non-AUG start codons. *Mol. Cell Biol.* 31, 4814–4831
46. Hinnebusch, A.G. (2005) Translational regulation of GCN4 and the general amino acid control of yeast. *Annu. Rev. Microbiol.* 59, 407–450
47. Kozak, M. (1991) Effects of long 5' leader sequences on initiation by eukaryotic ribosomes *in vitro*. *Gene Expr* 1, 117–125
48. Donahue, T. *et al.* (2000) Genetic approaches to translation initiation in *Saccharomyces cerevisiae*. In *Translational Control of Gene Expression* (Sonenberg, N., ed.), pp. 487–502, Cold Spring Harbor Laboratory Press
49. Algire, M.A. *et al.* (2005) Pi release from eIF2, not GTP hydrolysis, is the step controlled by start-site selection during eukaryotic translation initiation. *Mol. Cell* 20, 251–262
50. Hussain, T. *et al.* (2016) Large-scale movements of IF3 and tRNA during bacterial translation initiation. *Cell* 167, 133–144.e13
51. Yamamoto, H. *et al.* (2016) 70S-scanning initiation is a novel and frequent initiation mode of ribosomal translation in bacteria. *Proc. Natl. Acad. Sci. U. S. A.* 113, E1180–E1189
52. Qin, D. *et al.* (2007) Characterization of 16S rRNA mutations that decrease the fidelity of translation initiation. *RNA* 13, 2348–2355
53. Coureux, P.D. *et al.* (2016) Cryo-EM study of start codon selection during archaeal translation initiation. *Nat. Commun.* 7, 13366
54. Shin, B.S. *et al.* (2011) Initiation factor eIF2 promotes eIF2-GTP-Met-tRNA(i)(Met) ternary complex binding to the 40S ribosome. *Nat. Struct. Mol. Biol.* 18, 1227–1234
55. Hinnebusch, A.G. (2006) eIF3: a versatile scaffold for translation initiation complexes. *Trends Biochem. Sci.* 31, 553–562
56. Valášek, L. *et al.* (2001) Related eIF3 subunits TIF32 and HCR1 interact with an RNA recognition motif in PRT1 required for eIF3 integrity and ribosome binding. *EMBO J.* 20, 891–904
57. Valášek, L. *et al.* (2003) The yeast eIF3 subunits TIF32/a and NIP1/c and eIF5 make critical connections with the 40S ribosome *in vivo*. *Genes Dev.* 17, 786–799

58. Pisarev, A.V. *et al.* (2008) Ribosomal position and contacts of mRNA in eukaryotic translation initiation complexes. *EMBO J.* 27, 1609–1621
59. Khoshnevis, S. *et al.* (2014) Structural integrity of the PCI domain of eIF3a/TIF32 is required for mRNA recruitment to the 43S pre-initiation complexes. *Nucleic Acids Res.* 42, 4123–4139
60. Elantak, L. *et al.* (2007) Structure of eIF3b-RRM and its interaction with eIF3j: structural insights into the recruitment of eIF3b to the 40S ribosomal subunit. *J. Biol. Chem.* 282, 8165–8174
61. Elantak, L. *et al.* (2010) The indispensable N-terminal half of eIF3/HCR1 cooperates with its structurally conserved binding partner eIF3b/PRT1-RRM and with eIF1A in stringent AUG selection. *J. Mol. Biol.* 396, 1097–1116
62. Cuchalova, L. *et al.* (2010) The RNA recognition motif of eukaryotic translation initiation factor 3g (eIF3g) is required for resumption of scanning of posttermination ribosomes for reinitiation on GCN4 and together with eIF3i stimulates linear scanning. *Mol. Cell Biol.* 30, 4671–4686
63. Liu, Y. *et al.* (2014) Translation initiation factor eIF3b contains a nine-bladed beta-propeller and interacts with the 40S ribosomal subunit. *Structure* 22, 923–930
64. Erzberger, J.P. *et al.* (2014) Molecular architecture of the 40S-eIF3 translation initiation complex. *Cell* 158, 1123–1135
65. Hermannova, A. *et al.* (2012) Structural analysis of an eIF3 subcomplex reveals conserved interactions required for a stable and proper translation pre-initiation complex assembly. *Nucleic Acids Res.* 40, 2294–2311
66. Wei, Z. *et al.* (2006) Crystal structure of the C-terminal domain of *S. cerevisiae* eIF5. *J. Mol. Biol.* 359, 1–9
67. Siridechadilok, B. (2005) Structural roles for human translation factor eIF3 in initiation of protein synthesis. *Science* 310, 1513–1515
68. Srivastava, S. *et al.* (1992) Eukaryotic initiation factor 3 does not prevent association through physical blockage of the ribosomal subunit-subunit interface. *J. Mol. Biol.* 220, 301–304
69. Zhou, M. *et al.* (2008) Mass spectrometry reveals modularity and a complete subunit interaction map of the eukaryotic translation factor eIF3. *Proc. Natl. Acad. Sci. U. S. A.* 105, 18139–18144
70. Sun, C. *et al.* (2011) Functional reconstitution of human eukaryotic translation initiation factor 3 (eIF3). *Proc. Natl. Acad. Sci. U. S. A.* 108, 20473–20478
71. Querol-Audi, J. *et al.* (2013) Architecture of human translation initiation factor 3. *Structure* 21, 920–928
72. Masutani, M. *et al.* (2007) Reconstitution reveals the functional core of mammalian eIF3. *EMBO J.* 26, 3373–3383
73. Smith, M.D. *et al.* (2013) Human-like eukaryotic translation initiation factor 3 from *Neurospora crassa*. *PLoS One* 8, e78715
74. Smith, M.D. *et al.* (2016) Assembly of eIF3 mediated by mutually dependent subunit insertion. *Structure* 24, 886–896
75. Dong, Z. *et al.* (2013) Spectrin domain of eukaryotic initiation factor 3a is the docking site for formation of the a:b:i subcomplex. *J. Biol. Chem.* 288, 27951–27959
76. LeFebvre, A.K. *et al.* (2006) Translation initiation factor eIF4G-1 binds to eIF3 through the eIF3e subunit. *J. Biol. Chem.* 281, 22917–229132
77. Villa, N. *et al.* (2013) Human eukaryotic initiation factor 4G (eIF4G) protein binds to eIF3c, -d, and -e to promote mRNA recruitment to the ribosome. *J. Biol. Chem.* 288, 32932–32940
78. Yu, Y. *et al.* (2011) Common conformational changes induced in type 2 picornavirus IRESs by cognate trans-acting factors. *Nucleic Acids Res.* 39, 4851–4865
79. Marintchev, A. *et al.* (2009) Topology and regulation of the human eIF4A/4G/4H helicase complex in translation initiation. *Cell* 136, 447–460
80. Kumar, P. *et al.* (2016) Toward the mechanism of eIF4F-mediated ribosomal attachment to mammalian capped mRNAs. *Genes Dev.* 30, 1573–1588
81. Aylett, C.H. *et al.* (2015) Structure of a yeast 40S-eIF1-eIF1A-eIF3-eIF3j initiation complex. *Nat. Struct. Mol. Biol.* 22 (3), 269–271
82. Kouba, T. *et al.* (2012) Small ribosomal protein RPS0 stimulates translation initiation by mediating 40S-binding of eIF3 via its direct contact with the eIF3a/TIF32 subunit. *PLoS One* 7, e40464
83. Szamecz, B. *et al.* (2008) eIF3a cooperates with sequences 5' of uORF1 to promote resumption of scanning by post-termination ribosomes for reinitiation on GCN4 mRNA. *Genes Dev.* 22, 2414–2425
84. Munzarova, V. *et al.* (2011) Translation reinitiation relies on the interaction between eIF3a/TIF32 and progressively folded cis-acting mRNA elements preceding short uORFs. *PLoS Genet.* 7, e1002137
85. Nielsen, K.H. *et al.* (2006) Interaction of the RNP1 motif in PRT1 with HCR1 promotes 40S binding of eukaryotic initiation factor 3 in yeast. *Mol. Cell Biol.* 26, 2984–2998
86. Fraser, C.S. *et al.* (2007) eIF3j is located in the decoding center of the human 40S ribosomal subunit. *Mol. Cell* 26, 811–819
87. Chiu, W.L. *et al.* (2010) The C-terminal region of eukaryotic translation initiation factor 3a (eIF3a) promotes mRNA recruitment, scanning, and, together with eIF3j and the eIF3b RNA recognition motif, selection of AUG start codons. *Mol. Cell Biol.* 30, 4415–4434
88. Jivotovskaya, A.V. (2006) Eukaryotic translation initiation factor 3 (eIF3) and eIF2 can promote mRNA binding to 40S subunits independently of eIF4G in yeast. *Mol. Cell Biol.* 26, 1355–1372
89. Mitchell, S.F. *et al.* (2010) The 5'-7-methylguanosine cap on eukaryotic mRNAs serves both to stimulate canonical translation initiation and block an alternative pathway. *Mol. Cell* 39, 950–962
90. Aitken, C.E. *et al.* (2016) Eukaryotic translation initiation factor 3 plays distinct roles at the mRNA entry and exit channels of the ribosomal preinitiation complex. *Elife* 5, e20934
91. Simonetti, A. *et al.* (2016) eIF3 peripheral subunits rearrangement after mRNA binding and start-codon recognition. *Mol. Cell* 63, 206–217
92. Saini, A.K. *et al.* (2014) Eukaryotic translation initiation factor eIF5 promotes the accuracy of start codon recognition by regulating Pi release and conformational transitions of the preinitiation complex. *Nucleic Acids Res.* 42, 9623–9640
93. Pisareva, V.P. *et al.* (2008) Translation initiation on mammalian mRNAs with structured 5'-UTRs requires DExH-box protein DHX29. *Cell* 135, 1237–1250